

Reduction responsive superparamagnetic iron oxide nanoparticle clusters for T₂-T₁ magnetic resonance imaging

Bakr Abdullah Abdulhalim Noor

A Thesis
in
The Department
of
Chemistry and Biochemistry

Presented in Partial Fulfillment of the Requirements
for the Degree of Master of Science (Chemistry) at
Concordia University
Montreal, Quebec, Canada

April 2023

© Bakr Abdullah Abdulhalim Noor, 2023

CONCORDIA UNIVERSITY

School of Graduate Studies

This is to certify that the thesis prepared

By: Bakr Abdullah Abdulhalim Noor

Entitled: **Reduction responsive paramagnetic iron oxide nanoparticle clusters for T₂-T₁ magnetic resonance imaging** and submitted in partial fulfillment of the requirements for the degree of

Master of Science (Chemistry)

complies with the regulations of the university and meets the accepted standards with respect to originality and quality.

Signed by the final Examining Committee:

_____ Chair
Dr. Brandon Findlay

_____ Examiner
Dr. Zhibin Ye

_____ Examiner
Dr. Rafik Naccache

_____ Supervisor
Dr. John Oh

Approved by _____ Chair of Department or Graduate Program Director
Dr. Louis Cuccia

and _____ Dean of Faculty April/15/2023
Dr. Pascale Sicotte

Abstract

Reduction responsive superparamagnetic iron oxide nanoparticle clusters for T₂-T₁ magnetic resonance imaging

Bakr Abdullah Abdulhalim Noor

The main objective of this M.Sc. research is to synthesize a novel stimuli-responsive (SR) poly(acrylic acid) (PAA)-stabilized ultra-small superparamagnetic iron oxide nanoparticle (USNP) clusters as a switchable T₂-T₁ contrast agent for magnetic resonance imaging (MRI). Oleic acid (OA)-stabilized USNPs were synthesized in an organic solvent and their biphasic ligand exchange with an aqueous PAA solution yielded an aqueous dispersion of PAA stabilized USNP colloids (called PAA-USNPs) with the hydrodynamic diameter of ≤ 20 nm. The former colloids reacted with cystamine (Cys) to form disulfide-labeled PAA-USNP clusters with a diameter of >100 nm through the formation of amide linkages between terminal amino groups of Cys and carboxylic acid groups on the PAA-USNP. The resultant clusters reverted to individual PAA-USNPs with a hydrodynamic diameter close to that (≤ 20 nm) of PAA-USNPs upon the cleavage of disulfide bonds in the presence of a reducing agent such as dithiothreitol or glutathione. These SR PAA-USNP clusters have promising functions as an effective T₂-T₁ contrast agent. It can be anticipated that these PAA-USNPs and their clusters could find potential biomedical applications for the dual monitoring of T₁ and T₂ contrast using MRI of the bladder.

Acknowledgement

I would like to express my deepest thanks to my supervisor, Dr. Jung Kwon Oh for his continual support during my M.Sc's research and education. His encouragement, advice, and academic knowledge assisted me greatly during my program and aided in overcoming various challenges. His guidance as a supervisor helped advance my abilities as a researcher and my critical thinking. He has been of monumental help in my thesis revision and provided valuable feedback required, otherwise the process would have been far more arduous. I owe him a great debt for helping me develop into a better version of myself in the scientific field.

I'd like to kindly thank my committee members, Dr. Rafik Naccache, and Dr. Zhibin Ye, for their suggestions and guidance during various committee meetings. They helped provide additional unique points of view to my research and their advice was pivotal in improving my research. I'd also like to further thank Dr. Louis Cuccia, and Dr. Rafik Naccacche for offering to assist with the revision of my thesis. Their shows of kindness were highly appreciated and did not go unnoticed.

I'd also like to extend my thanks to Dr. Marc-André Fortin and Samila from the university of Laval. Their open door policy and willingness to assist with the characterization of my samples using equipment otherwise unavailable to me was highly appreciated.

No one could have welcomed me better nor made me feel more at home in the lab more so than my fellow group members. A special thanks and shoutout to Arman, Chaitra, Gandhi, Ge, Hourieh, Kamal, Kay, Twinkal, Sofia, and Xiaolei for showing me the ropes, advising me on my project, and most importantly for being my friends. My time at Concordia University would not have been the same without them.

Finally, I would like to thank my parents, Abdullah and Nahid, for their unwavering support in my education and believing in me and my best friend Wajid for his moral support and guidance. The continual assistance of my friends and family helped me see my M.Sc through to completion. Words are insufficient in expressing my gratitude to them.

Contribution of Authors

The bulk of the research in this thesis was conducted independently by myself under the sole supervision of Dr. Oh, , except for TEM measurements for fabricated PAA-USNP clusters before and after degradation were conducted by Ms. Sofia Papova (PhD student) in Dr. Oh's laboratory.

Contents

List of Figures	vii
List of abbreviations	x
Chapter 1: Introduction	1
1.1 General background of magnetic resonance imaging (MRI)	1
1.2 General background for MRI contrast agents (CAs)	4
1.2.1 Paramagnetic CAs	6
1.2.2 Superparamagnetic CAs	8
1.3 Stabilization of SNPs	11
1.3.1 Acidic surfactants	12
1.3.2 Inorganic surfactants	14
1.3.3 Polymeric stabilizers	16
1.4 Synthesis of colloidal SNPs	23
1.4.1 Co-precipitation	23
1.4.2 Thermal decomposition	24
1.4.3 Polyol method	25
1.5 Stimuli-responsive nanoparticles for MRI	26
1.6 Scope of this thesis	32
Chapter 2: Experimental	33
2.1 Instrumentation and analyses	33
2.2 Materials	34
2.3 Synthesis of OA-Stabilized USNPs	34
2.4 Fabrication of PAA-USNPs via ligand exchange	35
2.5 Fabrication of SR PAA-USNP clusters by coupling reactions	35
2.6 Reductive degradation of PAA-USNP clusters	35
Chapter 3 Synthesis and reductive degradation of PAA-USNP clusters	36
3.1 OA-Stabilized USNPs (OA-USNPs)	36
3.2 Fabrication of PAA-stabilized USNPs via biphasic ligand exchange	38
3.2.1 Effect of molecular weight of PAA on ligand exchange	44
3.3 Synthesis of SR PAA-USNP clusters via EDC coupling	45
3.4 Reductive degradation of SR PAA-USNP clusters	49
Chapter 4 Conclusion and Future Work	51
References:	52

List of Figures

Figure 1 Shown in a) and b) are images sensitive to two different contrast types. a) An image sensitive to T_1 contrast, while b) is an image sensitive to T_2 contrast. Note that although much of the same brain structure is present in both images the relative intensities of different tissue types are very different⁴.

Figure 2 Groups that can be used to anchor polymers on SNP surfaces.

Figure 3 A scheme describing the functionalization of SNPs. Steps 1A and 1B: ligand exchange reactions. Step 2: acylation of hydroxyl groups to prepare ATRP surface initiators. Step 3A: surface-initiated ring opening polymerization of L-lactide. Step 3B: surface initiated ATRP. Step 4: deprotection or additional reaction after polymerization. Step 5: grafting of end functionalized PEG chains onto the nanoparticle surface using amidation chemistry⁵⁸.

Figure 4 Formation of a) Magnetic beads and b) colloidal nanocrystals due to the presence of PVA⁷⁰.

Figure 5 Chitosan stabilized SNPs³⁸.

Figure 6 Schematic illustration of the fabrication of DOX-loaded magnetic star-shaped polymer micelles⁹³.

Figure 7 Schematic illustration of nanodrug preparation and dual-sensitive SF release in HepG2 cells⁹⁴.

Figure 8 ESNP clusters disassembling into individual ESNPs due to the acidic environment of a tumor⁹⁸.

Figure 9 Scheme for preparation of ESNPs-packaged poly(CBMA) nanogels

modified with c(RGD) ligand as an activatable MRI contrast agent with switchable.

function from a T_2 contrast agent to a T_1 one through the stimuli-responsiveness of

GSH¹⁰⁰.

Figure 10 a) DLS diagram in hexane, b) TEM image, c) TGA thermogram, and d) XRD of magnetite OA-USNPs.

Figure 11 Illustration of the biphasic ligand exchange utilized to fabricate PAA-USNPs, followed by their purification.

Figure 12 Illustration of biphasic ligand exchange utilized to fabricate PAA-USNPs using organic solvents a) chloroform b) hexane followed by their purification.

Figure 13 Illustration of fabricated PAA-USNP diameter decreasing ligand exchange with increased EtOH concentrations a) 16.5 %, b) 33 %, c) 66 %, and d) 82.5 %.

Figure 14 a) Schematic illustration of biphasic ligand exchange of OA-USNPs in hexane and PAA in aqueous phase, b) DLS diagram, c) TEM image, and d) TGA thermogram of PAA-USNP colloids.

Figure 15 DLS diagrams of PAA-USNPs fabricated with PAA whose molecular weight is a) 2000, b) 5000, and c) 8000 g/mol.

Figure 16 Illustration to fabricate SR PAA-USNP clusters through the formation of amide linkages by EDC coupling of Cys with PAA-USNPs.

Figure 17 DLS diagrams of PAA-USNP clusters fabricated by altering NH₂: COOH mole ratios to a) 0.32:1, b) 0.64:1, c) 1.28:1, and d) TEM image of PAA-USNP clusters.

Figure 18 DLS diagrams of PAA-USNP clusters with diameter of 60 nm a) before and b) after treatment with DTT, and c) TEM image of PAA-USNP clusters after DTT treatment.

List of abbreviations

ATRP	Atom transfer radical polymerization
CA	Contrast agent
Cys	Cystamine dihydrochloride
c(RGD)	Cyclo[Arg-Gly-Asp-D-Tyr-Lys]
DDA	Direct detection agents
DLS	Dynamic light scattering
DTT	Dithiothreitol
ESNP	Extremely-small superparamagnetic iron oxide nanoparticle
EtOH	Ethanol
GSH	Glutathione
Gd-DTPA	Gadolinium-diethylenetriamine-pentaacetic acid
HCC	Hepatocellular carcinoma
MPIO	Microparticles of iron oxides
MRI	Magnetic resonance imaging
MTT	3-(4,5-dimethylthiazol-2-yl)-2,5-diphenyltetrazolium bromide
NMR	Nuclear magnetic resonance
NaOH	Sodium hydroxide
OA	Oleic acid
PAA	Poly(acrylic acid)
PCL	Poly(caprolactone)
PD	Proton density
PEG	Poly(ethylene glycol)

PVA	Poly(vinyl alcohol)
RES	Reticuloendothelial system
RF	Radiofrequency
SNP	Superparamagnetic iron oxide nanoparticle
SR	Stimuli responsive
TE	Time to echo
TEM	Transmission electron microscopy
TGA	Thermogravimetric analysis
TMAOH	Tetramethylammonium hydroxide
TR	Repetition time
USNP	Ultra-small superparamagnetic iron oxide nanoparticle
XRD	X-ray diffraction
ZOL	Zoledronic acid

Chapter 1: Introduction

1.1 General background of magnetic resonance imaging (MRI)

While the advent of MRI in the 1970s was initially viewed as unpromising¹, the technology has evolved to become immensely sophisticated and a widely used clinical modality over the past 40 years². This popularity is in many parts due to their unique features, such as being non-invasive, painless, and radiation-free. Furthermore, MRI possesses high tissue sensitivity due to its utilization of strong magnetic fields to create detailed 2D and 3D images of the various tissues and organs present within the body³.

The basis of most modern MRI techniques are derived from nuclear magnetic resonance (NMR) with which it shares designs such as strong magnetic fields, a transmitter coil capable of providing energy to a sample, and a detector coil which serves to measure and read energy emitted to and back from the sample⁴. The potential of NMR usage in medicine was indicated thanks to a study by Damadian in 1971, this study measured T_1 & T_2 relaxation times of excised normal tissue as well as tumor tissues before concluding that tumor tissues had longer relaxation times than normal tissue⁴. It's also worth mentioning that different tissues have different T_1 & T_2 relaxation times. In a descending order, the value of T_1 and T_2 is highest in fluids, water-based tissues, and the lowest and fat-based tissues^{1,5}. But how are MR Images produced? Some information will be covered below to garner a basic understanding of the mechanisms and terminologies involved with the MRI.

The MRI utilizes proton density (PD) which is the amount of hydrogen atoms present within a specific volume of a region of interest; the abundant presence of hydrogen present in water or lipids within the body (up to 75% to 80%) is essential to the working of an MRI. When a radiofrequency (RF) pulse is emitted by MRI, protons within the water in the region of interest are excited when a magnetic field is applied. The time taken for them to relax is known as the spin-lattice relaxation time (T_1) & spin-spin relaxation time (T_2). These properties are just as important as PD for MRI^{1,5}.

We can summarize that the MRI can produce two contrasts, which are the T_1 & T_2 contrasts. When generating a T_1 contrast, fats are viewed brightly, watery tissues are grey, and fluids as extremely dark. In comparison, using T_2 contrast, fluids are viewed brightly, while fatty and watery tissues are mid-grey. What's important to note is that both T_1 and T_2 imaging relies on the properties of the tissue they scan, some of which can be more easily viewed in one mode over the other³.

In most cases, diseased or cancer tissue can be viewed and distinguished from healthy tissues in the MR Images, thanks to the intrinsic difference between their T_1 and T_2 properties. However, some pathological conditions aren't significantly different in morphology or relaxation measurements. This is where contrast agents come into play, by altering the relaxation times of the diseased tissue, contrast agents can play a significant role in distinguishing diseased tissues from their healthy counterparts and as a result enhance the image quality produced by the MRI⁶.

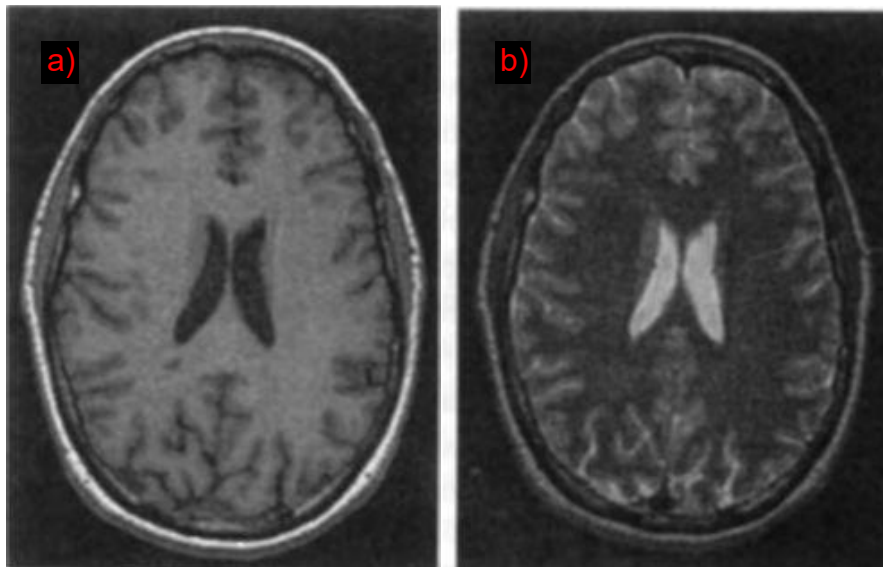


Fig 1. Shown in a) and b) are images sensitive to two different contrast types. a) An image sensitive to T_1 contrast, while b) is an image sensitive to T_2 contrast. Note that although much of the same brain structure is present in both images the relative intensities of different tissue types are very different⁴.

1.2 General background for MRI contrast agents (CAs)

Contrast agents (CAs) alter the relaxation times of tissues and thus potentially enhance the contrast quality produced by MRI. However, what influenced research into CAs in the first place?

This question can be in a large part credited to differing tissue compartments having differing relaxation rates thus spurring research into the topic in the 1970s to understand the mechanisms by which paramagnetic ions accelerated the magnetic relaxation of water protons. Of particular interest were paramagnetic ions such as Mn(II), lanthanide, and Gd(III) ions, all of which were utilized to alter *in vivo* MR properties. Through various experiments, it was determined that the use of paramagnetic ions in low concentrations enhanced image quality⁷. The very first paper published about CAs was by Hans Weinmann et al in 1984, which indicated the potential of gadolinium-diethylenetriamine-pentaacetic acid (Gd-DTPA) complex as a CA for the NMR and for the MRI if suitably developed⁸. With the history involving the advent of MRI CAs briefly covered, we can delve into greater details about the classifications and properties of CAs.

There are a few ways in which CAs are classified. Some of these will be mentioned before we further discuss each type of CAs their examples in greater detail. It is important to note, however, that these classifications denote the effect of CAs on relaxivity measurements in the MRI, while the other mode of classification specifies the CA's biophysical properties. Therefore, these modes of classification do not oppose each other.

One method of classification is dependent upon a CA's effects on the generation of an MRI contrast through relaxation times. CAs classified as T_1 -weighted CAs generally increase longitudinal relaxation rates ($1/T_1$) of water protons more so than the transverse relaxation rates ($1/T_2$), whereas T_2 CAs do the opposite of T_1 CAs and generally have a higher effect on the transverse relaxation rates^{9,10}.

Another means of classification is dependent upon the magnetic properties of the CAs in question or their biophysical mechanism of action. These include paramagnetic and superparamagnetic CAs which include Gadolinium based CAs as well as iron oxide based CAs respectively^{11,12}.

Relatively new CAs called chemical exchange saturation transfer (CEST), work by exchanging their pre-saturated exchangeable protons (such as NH, OH) with those of bulk water leading to a reduced signal intensity of water. They behave like MRI CAs as a result.^{10,11}

Another type of CAs are stable liposomal formulations of hydrophilic fluorinated molecules referred to as Direct Detection Agents (DDA)¹¹.

1.2.1 Paramagnetic CAs

Paramagnetic CAs have been and continue to be extensively researched. This makes them quite prominent if not the most prominent MRI CAs^{10,11}. These CAs include metal ions, organic free radicals, and other contrast agents possessing unpaired electrons^{9,13}. They are predominantly used as T₁ CAs due to their reduction/shortening of T₁ relaxation times¹⁴. Very prominent examples of these include but are not limited to lanthanide and transition metal ions such as gadolinium (Gd³⁺), manganese (Mn²⁺/Mn³⁺), lanthanide (La³⁺) and dysprosium (Dy³⁺). It's important to note, however, that paramagnetic CAs can behave as T₂ CAs, especially if their concentration is very high, as paramagnetic metal ions such as dysprosium (Dy³⁺) and holmium (Ho³⁺) present notable T₂ contrast enhancement¹⁵.

Gadolinium CAs (Gd³⁺) is a lanthanide ion with seven unpaired electrons. This asymmetry of the ion leads to very rapid electron spin relaxation aiding in MRI signal enhancement¹⁶. Despite the toxicity related to multivalent ion, the very first FDA-approved CA was the gadolinium based 'gadopentetate dimeglumine (Magnevist®)' in 1988. Since then, multiple gadolinium-based CAs have been commercialized^{16,17}. Lanthanide metal ions such as Gd³⁺ are toxic heavy metals, however, utilizing proper chelating ligands, Gd³⁺ can remain chelated in the body, prevent the dissociation of Gd³⁺, and be excreted intact^{14,16}, making them quite ideal as T₁ CAs. However, health concerns associated with the usage of gadolinium CAs emerged in various forms. Mounting evidence of this has caused concerns and re-regulations of the gadolinium contrast agents. Health associations such as the European Medicines Agency, the FDA, and Japan's Pharmaceuticals and Medical Devices all updated their policies regarding the commercially used Gadolinium CAs¹⁶.

These concerns began as early as 1996 when patients administered with gadolinium CAs showcased adverse reactions at a rate higher than anticipated (0.01% instead of 0.0003%)¹⁸.

Nephrogenic systemic fibrosis, a disease affecting patients with renal failure, was suspected to be linked to gadolinium CAs as early as 2006 and could cause extreme life threatening reactions¹⁹.

Despite allergic reactions being rare and most of them being mild, some reactions require immediate management^{20,21} and occur despite the use of premedication (corticosteroids and antihistamines) in patients^{22,23}.

The safety profile of gadolinium CAs from 2009 was largely restored until further evidence proved the deposition of gadolinium in the central nervous system in 2013 & 2014. In 2016 and 2018, further evidence of gadolinium accumulation in bones was discovered which lead to further concerns about the usage of gadolinium CAs^{11,23}.

1.2.2 Superparamagnetic CAs

Superparamagnetic CAs consist of colloidal materials made up of nanoparticles in a suspension, consisting of nonstoichiometric metal oxide cores¹¹. Typical superparamagnetic CAs are superparamagnetic iron oxide nanoparticles (SNPs), whose cores are composed of magnetite (Fe_3O_4) or maghemite ($\gamma\text{-Fe}_2\text{O}_3$)^{10,12,24,25}.

But why are iron oxide nanoparticles referred to as superparamagnetic? This is because in the bulk phase of iron oxide, the magnetization is the sum of all the magnetic moments which are present in the entire volume of the material. This bulk phase material is made up of multiple domains, each one having its own magnetic vector. When these vectors are not aligned there is a decrease in the magnetization, and when the size of the material is made smaller, or in this instance, brought to a nanoscale, the numbers of domain present decrease until a singular domain remains. The size that this occurs is called critical size. A magnetic material with only one domain is called superparamagnetic and this can be seen in iron oxide nanoparticles^{25,26}. As a result, SNPs have a magnetic moment that is far greater than that of paramagnetic substances, resulting in their specific magnetic susceptibilities to exceed those of soluble paramagnetic species and yet lack any magnetization unless an external magnetic field acts upon them²⁴. This means a lower dose of superparamagnetic CAs is required for MRI²⁷. For example, the recommended dose of ferumoxides is 0.05 mL/kg while the dose recommendation of Gd chelates for liver imaging is 0.2 mL/kg²⁸.

Furthermore, SNPs have an interesting size-dependent property which can alter their contrast enhancement properties. Based on their size they can function as either T₂-weighted CAs, or T₁-weighted CAs^{29,30}. There are three common terminologies used to describe them: i) SNPs which have diameters > 10-30 nm act as T₂-weighted CAs. ii) ultras-small-SNPs (USNPs) with less than 10 nm in diameter act as T₁-weighted CA and, iii) extremely-small SNPs (ESNPs) with < 3 nm diameter as excellent T₁-weighted CA^{1,25,30}. This property has increased the potential applications of iron oxides as CAs.

These properties assisted in the conception of iron oxides as CAs. This was seen when dextran-magnetite was put forward as a potential T₂ relaxation reagent with use in gels for the NMR in 1978³¹. Their potential use as T₂ MRI CAs weren't yet discussed until 1982 when Wolf et al demonstrated their use via signal reduction in the liver and spleen. Their use *in vivo* wasn't uncommon as colloidal dextran-stabilized iron(III) oxide solutions had been long-established injectable drugs⁷.

This would inevitably lead to further research on the possible usage of SNPs as CAs. Success in this was followed by the approval of the FDA and EMA resulting in clinical production of multiple inorganic iron oxide nanoparticles as CAs. Feridex® & Endorem® (1996), Lumirem® (1996), Resovist® (2001), and Sinerem® (2007) are examples of the commercialized iron oxide CAs with applications in the imaging of liver lesions, bowel imaging enhancement and lymph node metastases imaging^{12,32}.

Some of the factors behind the discontinuation of these CAs could be attributed to iron oxide CAs not being widespread clinically because of a lack of clinical knowledge to interpret iron oxide enhanced MR images when compared to their Gd counterparts, which are widely spread³³. Furthermore, iron oxide CAs would be mostly useful for patients with renal deficiencies who are otherwise unable to use gadolinium CAs. Due to the small population of these patients, there is a low financial incentive for pharmaceutical companies to develop iron oxide CAs³³. Another factor to consider is that SNPs, especially those acting as T₂ CAs can cause a large decrease in signal intensity resulting in an image distortion causing a decrease in image quality referred to as “Blooming”²⁴. These factors were closely tied in with the use of iron oxide as T₂-weighted CAs, as research pertaining the use of iron oxide as T₁-weighted CAs shows great promise²⁴ which can be seen by the extensive research still conducted on SNPs.

Iron oxide CAs have advantages that merit their use and research. Many studies indicate that in comparison to paramagnetic CAs such as gadolinium, iron oxide CAs are far less toxic due to the labile presence of iron within the body. In fact, lysosomes can convert them into non-magnetic iron ions useable in the hemoglobin, and so on³². No life-threatening adverse effects have been recorded from the use of SNP CAs which have become some of the most preferable nanomaterials in medical sciences. This is due to their features of minimal toxicity and biocompatibility³⁴. This can be further seen in a study conducted by Jain et al in 2008 where 10 mg Fe/Kg was administered to rats to determine the biodistribution, clearance and biocompatibility of iron oxide nanoparticles. The study indicated that no long-term effects were caused³⁵.

1.3 Stabilization of SNPs

For most nanoparticles to be used, they are dispersed in a liquid phase allowing for these nanoparticle suspensions to be utilized³⁶. However, naked magnetic nanoparticles face multiple limitations. Their surfaces are hydrophobic which means they can't be easily dispersed in an aqueous phase. Uncoated nanoparticles can interact with particles in biological media resulting in toxicity and aggregation. Uncoated SNPs can be easily oxidized when their surfaces are exposed to oxygen thus leading to a loss of magnetization. Furthermore, uncoated magnetic nanoparticles, when exposed to MRI's magnetic field, can come in contact with their neighbors' magnetic field resulting in attraction, additional enhancement of magnetization, and further increase chances of aggregation^{37,38,39,40}.

To summarize, SNPs and other biomedical nanoparticles are affected by a variety of forces that can impact their stability. These include i) van der Waal's forces, ii) electrostatic repulsive forces, iii) anisotropic interactions, and iv) steric repulsive forces. All these factors need to be controlled for the stability of nanoparticles⁴⁰.

For all of this to be achieved, that is, to improve the colloidal stability of nanoparticles such as SNPs, surface coatings are required³⁸. There are various surfactants that are used to coat the surfaces of nanoparticles. Typical surfactants include monomeric stabilizers, inorganic materials, and polymeric stabilizers⁴⁰. All of which have their own advantages and limitations.

The main focus of this segment will be to preview conventionally used surfactants for SNPs.

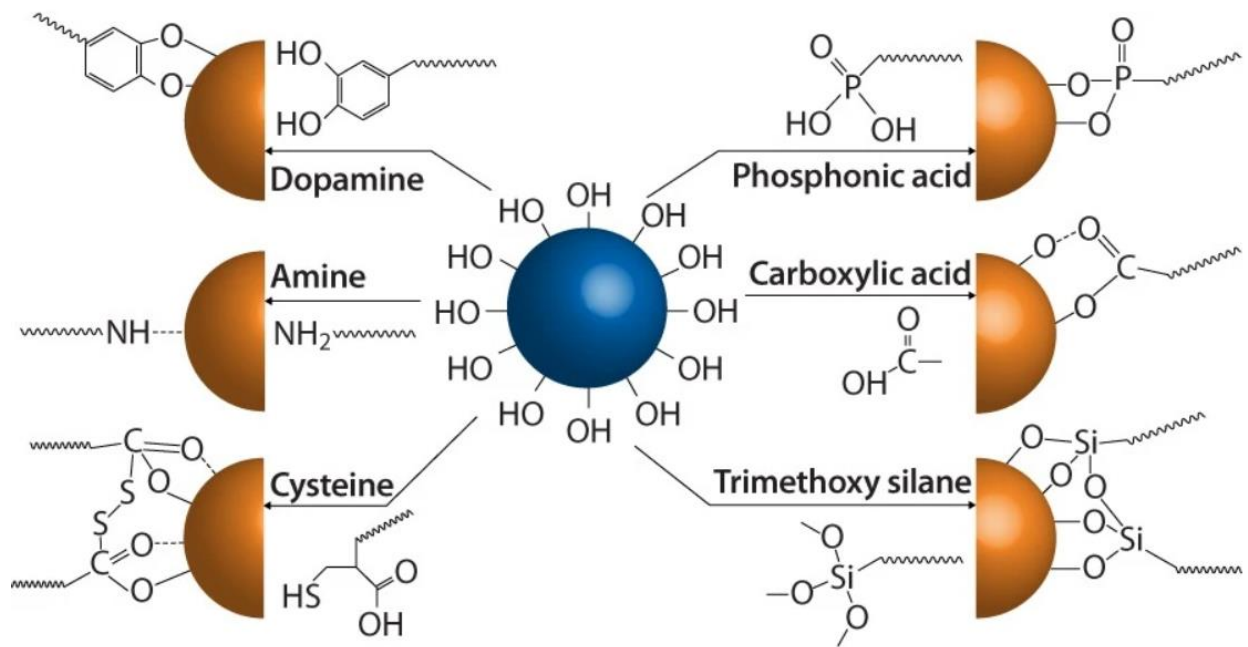


Fig 2. Groups that can be used to anchor polymers on SNP surfaces.

1.3.1 Acidic surfactants

A variety of surfactants labelled with acidic anchoring groups, typically, phosphates and carboxylates are called acidic surfactants as seen in Fig 2. They allow for translation of SNPs into aqueous media⁴⁰, imparting functionality and conjugation with biologically active agents⁴¹. Certain acidic polymers and molecules based on fatty acids provide additional advantages such as colloidal stability and terminal functional carboxyl groups, while poly(acrylic acids) increase the stability and biocompatibility of the nanoparticles as well as aid in bio adhesion³⁷.

Beyond the stability, the functional coating/surfactant can be used to allow the attachment of foreign molecules such as proteins, glycoproteins, oligonucleotides and other ligands on the surface via covalent binding^{37,42}. This occurs by the adsorption of the acid on the surface of the magnetite nanoparticles, depending on the surface of the nanoparticle as well as the type of acid

used. It leaves at least one functional group exposed to the solvent which allows the surface to become hydrophilic as well as allow the attachment of molecules to the functional group⁴⁰.

While these coatings allow for the stabilization of SNPs in aqueous media, they have some limitations. Their stability is dependent upon the concentration of acidic surfactants adsorbed on their surfaces while being sensitive to pH fluctuation^{40,43} which can occur in a biological system. Furthermore, the co-ordination bond between the -COOH surfactants and SNPs surface is labile. A concern is that the surfactants can be dissolved upon the elevation of the nanoparticle's surface temperature or can be replaced. Phosphonic acids that have a stronger affinity to SNP surfaces is through the formation of -Fe-O-P bonds⁴⁴.

We briefly overlook some stabilizations of SNPs with different acidic surfactants. Luanne et al. explored carboxylic acid surfactants (tiopronin, oxamic acid and succinic acid) via co-precipitation, resulting in the formation of stabilized SNPs (<10 nm) dispersed in aqueous solutions with antibacterial properties using magnetic hypothermia⁴⁵. Paula et al. stabilized SNPs (< 9 nm) with oleic acid (OA) and noted the surfactant's influence on the magnetic property of the nanoparticle where OA could lower the saturation magnetization of the SNPs at a suitable concentration⁴⁶. Furthermore, SNPs stabilized with citric acid have been commercialized and are called VSOP-C184. It had a diameter of 7.0 ± 0.15 nm and achieves high T_1/T_2 ratios, thus being an effective T_1 CA^{44,47}. Yee et al. reported the stabilization of SNPs (<10 nm) with alkanesulfonic and octadene phosphonic acid through a one-phase synthesis⁴⁸.

All this indicates that the selection of a suitable surfactant is a matter of broad research which can be complicated as new surfactants continue to be developed. Further research is required to compare the advantages and disadvantages/limitations between the multitude of already available surfactants compared to one another, their synergy with the type of nanoparticle to be coated as well as the systems in which they are intended to be used for before an ideal surfactant is picked for the nanoparticle's function.

1.3.2 Inorganic surfactants

Like the name suggests, the process to stabilize SNPs with inorganic materials involves the coating of an SNP with an outer metallic shell composed of inorganic materials⁴⁰ such as silica, gold, gadolinium, platinum etc⁴⁰. Inorganic surfactants provide SNPs with colloidal stability in a solution while also providing a method to bind various biological ligands to the nanoparticle's surface^{37,40}. However possess rather large limitation such as inorganic surfactants is that the magnetic nanoparticles prepared for drug delivery/in-vivo applications require them to be biocompatible meaning that so does the metallic surfactant³⁷.

Silica coating has been used to stabilize SNPs by shielding their magnetic dipole interactions and to aid in the repulsion of SNPs from one another, thus preventing aggregation⁴⁰. Furthermore, a silica nanoparticle was approved by the FDA for clinical human testing to be utilized in cancer imaging⁴⁹. If these trials succeed, it could potentially increase research of nanoparticles stabilized by silica. Several reports discussed Silica surfactants with their means of production and means by which they are coated around an iron oxide nanoparticle. Masoud et al classified silica coated

SNPs in two ways: i) Nonporous silica coatings, and ii) Porous silica coatings³⁸ depending on the type of silica used to coat the nanoparticles.

Silica can be applied onto the surface of nanoparticles in multiple ways. Typical methods include i) The Stöber process⁵⁰ and ii) reverse-microemulsion techniques^{51,52}. The Stöber process forms a silica nano-shell around a seed of the material to be encapsulated utilizing hydrolysis and condensation of sol-precursor⁵².

The Stöber process utilizes aqueous alcohol solutions typically composed of methanol and ethanol for its reactions. Thus, hydrophobic nanoparticles need to be made hydrophilic via processes such as ligand exchange for effective participation in the Stöber coating reactions⁵².

This can be a significant limitation. Newer methods such as reverse-microemulsion can be used to coat both hydrophilic and hydrophobic nanoparticles with silica. It does this inside micelles by confining metal seeds of the desired nanoparticle and depositing silica on them⁵².

When coating metal surfactants on top of SNPs, there are two general ways utilized and these are the direct reduction of single-metal ions on the SNP surface while the most common method involves the reduction of singular metallic ions on an already existing surfactant which might be a small molecule, polymer, silica or other functionalized SNPs⁵¹. A novel iron oxide core capped with gold was synthesized utilizing two steps, which is the formation of SNPs coated with silica followed by the addition of gold atop the nanoparticle using the growth method⁵³. Another study showcased SNPs coated with a carboxylate platinum (IV) and compared it with SNPs functionalized with a platinum(II) complex functionalized with dextran to test the colloidal

stability of the nanoparticles⁵⁴. Similarly, SNPs coated with silica were produced by thermal decomposition and aminated to which Gd-DTPA complexes were conjugated for use as a unique T₁ & T₂ dual contrast agent in the MRI⁵⁵. The possibility of adding additional properties of metals onto the contrast agent dramatically increases the scope of SNPs in biomedical and catalytical applications⁵¹.

1.3.3 Polymeric stabilizers

Polymeric stabilizers offer an extremely large variety of stabilizers or surfactants for nanoparticles including SNPs. Most studies, up until recently, have not been focused on polymer functionalized iron oxides, but this has changed due to the advantages that polymeric surfactants/stabilizers can provide the SNPs⁵¹. These coatings can be applied *in situ* such as through co-precipitation, post synthesis⁴⁰, atom transfer radical polymerization (ATRP) for polymeric shells with low polydispersity⁵¹, and ligand exchange^{56,57}. Some of the methods that allow for the stabilization of SNPs with polymeric stabilizers are depicted in Fig 3. This section describes examples of polymeric stabilizers of SNPs. Including poly(ethylene glycol) (PEG), dextran, poly(vinyl alcohol) (PVA), chitosan and alginate.

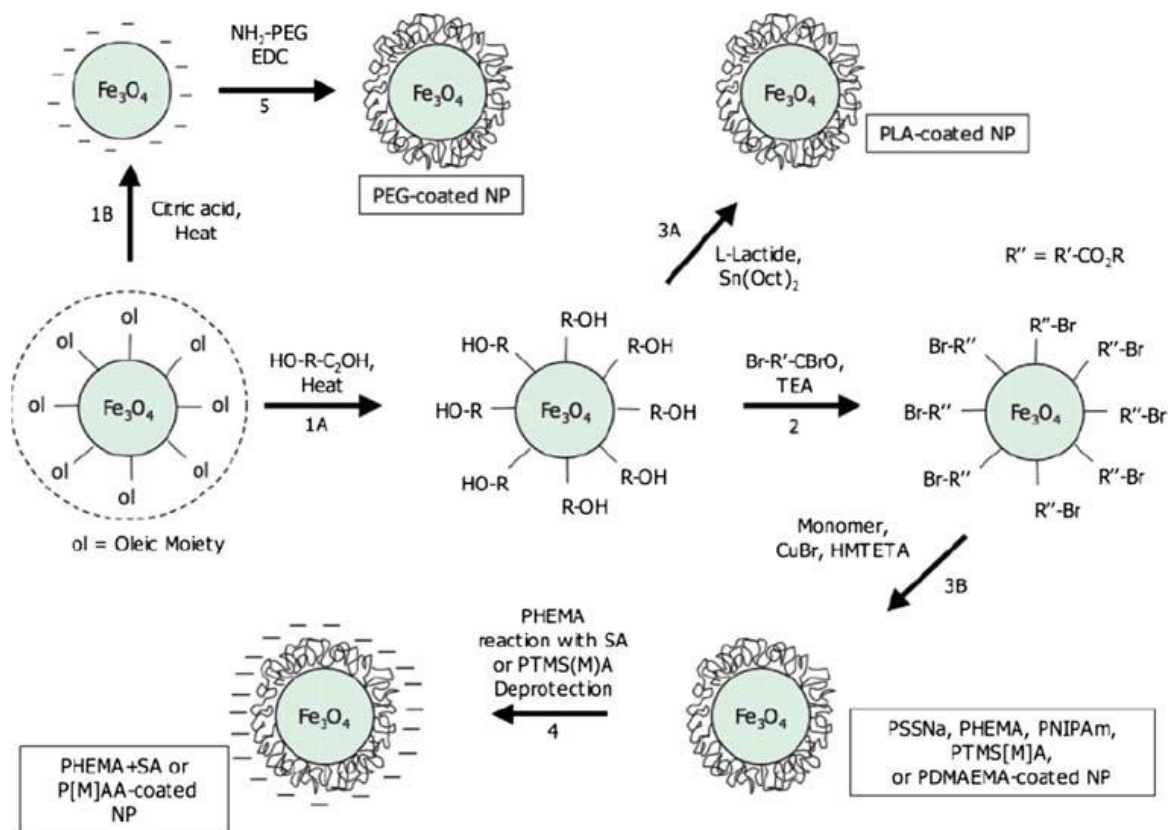


Fig 3. A scheme describing the functionalization of SNPs. Steps 1A and 1B: ligand exchange reactions. Step 2: acylation of hydroxyl groups to prepare ATRP surface initiators. Step 3A: surface-initiated ring opening polymerization of L-lactide. Step 3B: surface initiated ATRP. Step 4: deprotection^{38,40,51} or additional reaction after polymerization. Step 5: grafting of end functionalized PEG chains onto the nanoparticle surface using amidation chemistry.⁵⁸

PEG is a hydrophilic, water-soluble, biocompatible polymer with low toxicity to cells and long-term stability^{38,40,51}. PEG also possesses nonantigenic and non-immunogenic properties⁵⁹. PEG has been known to minimize non-specific interactions with serum proteins. Thus, PEG has been extensively used to form shells around nanomaterials to improve their steric stability *in vivo*. This provides prolonged circulation in blood and reduced reticuloendothelial system (RES) uptake⁵⁹. Due to these features, PEG has also been explored as a biocompatible stabilizer for

SNPs. Several reports studied the effects of molecular weights of PEG on half-life of PEG-stabilized SNPs. These studies suggest the higher the PEG molecular weight, the longer the half-life^{60,61,62}. For example, Xue et al experimentally demonstrated that the half clearance time of PEG during blood circulation can increase from 30 minutes to 24 hours with an increase of PEG molecular weight from a few thousands to a few hundred thousands⁶⁰. Other reports describe robust methods of PEG coatings on SNPs for their use in MRI with other biomedical applications^{63,64}.

Dextran is a polysaccharide composed of α -D-glucopyranosyl units with a varying degree of chain length and units⁴⁰. The main benefit of using dextran as a polymer surfactant on nanoparticles is due to its biocompatibility and improved blood circulation time of coated nanoparticles as well as its optimum polar interactions with iron oxide surfaces^{38,40,51,59}.

A study conducted to find the biocompatibility of dextran showed that it is quite stable in most tissue environments. This is mainly because while some bacterial enzymes can degrade dextran, these enzymes aren't produced by tissues^{37,65,66}. A limitation faced by commonly used dextran coated nanoparticles is that they do not undergo extensive cellular uptake which can prevent some biomedical uses such as cell tracking. However, a method to overcome this limitation could be the coupling of the dextran surfactant with specific ligands³⁷. A study by Josephson et al showcased that by the attachment of a small peptide known to facilitate cell internalization on the surface of the dextran nanoparticles significantly improved their internalization^{37,67}.

PVA is a hydrophilic and biocompatible polymer which has excellent film forming, emulsifying and adhesive properties^{40,59}. Coating nanoparticles with PVA prevents their agglomeration and gives rise to monodisperse particles^{37,40,51,59}.

The cytotoxicity of PVA-coated SNPs was compared with those of uncoated SNPs in mouse fibroblast cell lines (L929) using an 3-(4,5-dimethylthiazol-2-yl)-2,5-diphenyltetrazolium bromide (MTT) assay. The results indicate that PVA SNPs with concentrations as high as 400 mM over 72 hours demonstrated acceptable levels of cell viability when compared to their uncoated counterparts under the same conditions⁶⁸. Furthermore, PVA coated SNPs were studied as potential magnetic carriers owing to their ease of functionalization. They were conjugated with doxorubicin to explore their drug loading and release profiles. Up to 45% of the adsorbed drug was released within 80 hours. These results suggest that PVA-coated SNPs promising for use as magnetic drug carriers in magnetically targeted drug delivery⁶⁹. Methods to synthesize PVA stabilized SNPs have also been explored in a variety of ways. Mahmoudi et al. explored the formation of uniform spherical SNPs, nanorods, magnetic beads and colloidal nanocrystal clusters using PVA via an aqueous coprecipitation process (Fig 4)⁷⁰. Chastellain et al. explored the synthesis of ferrofluids through a multistep synthesis before grafting them with PVA to ensure their colloidal stability⁷¹.

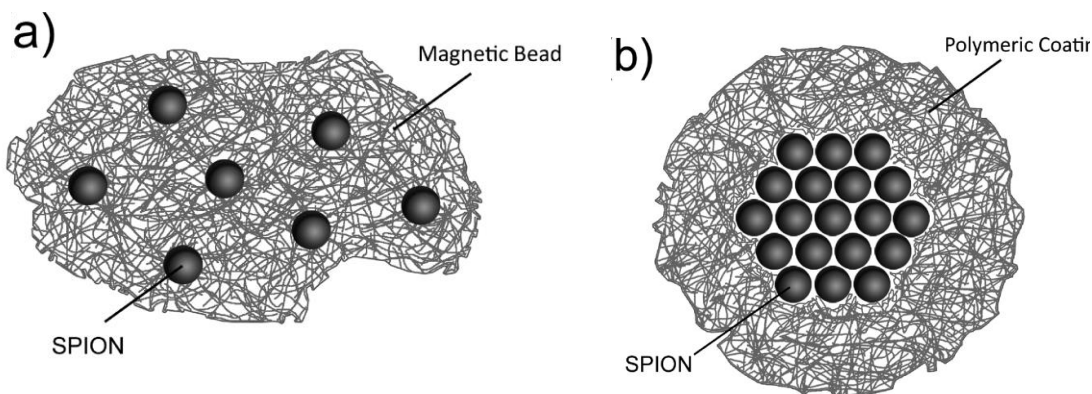


Fig 4. Formation of a) Magnetic beads and b) colloidal nanocrystals due to the presence of PVA⁷⁰

Chitosan is a naturally occurring cationic polymer which has garnered significant interest as a surfactant for nanoparticles due to its hydrophilicity as well as biocompatibility, furthermore, it can stabilize nanoparticles and prevents agglomeration thus creating a monodisperse population of nanoparticles^{40,59}. As a result, chitosan is widely used in non-viral gene delivery systems, and can be further seen with uses in biotechnology, textiles, food, medicine, agriculture, textiles and water treatment^{37,51}.

This widespread use of the polymer potentially makes its application in the nanomedicine field quite appealing as can be seen in papers exploring the synthesis of nanoparticles stabilized with chitosan. For instance, gold nanoparticles were synthesized in the presence of chitosan which acted as both, a reducing agent as well as a stabilizer whose concentration could be altered to manipulate the gold nanoparticles' shape and size, furthermore, the chitosan could undergo gelation in the presence of tripolyphosphate to synthesize a bimodal sized distribution of particles including spherical and polygonal gold nanoparticles capped with chitosan⁷². Another paper used a novel method to synthesize monodispersed USNPs (3-5 nm in diameter) stabilized

with chitosan-polyacrylic acid nanospheres with potential use as T₂ contrast agents for the MRI⁷³. Multifunctionalized graphene sheets embedded with chitosan stabilized SNPs were also explored as potential theranostics for both gene and drug delivery, these showcased efficient drug loading capacity and pH dependent release with better cytotoxicity than free doxorubicin⁷⁴. The biocompatibility induced by chitosan was explored utilizing chitosan stabilized cobalt ferrite nanoparticles with the potential to work as T₂ contrast agents in the MRI where the nanoparticles underwent cytotoxicity tests conducted by administering the nanoparticles to rodents at dosages of 1-20 mg/kg bodyweight before the study concluded the doses as safe for male albino Wistar rats⁷⁵.

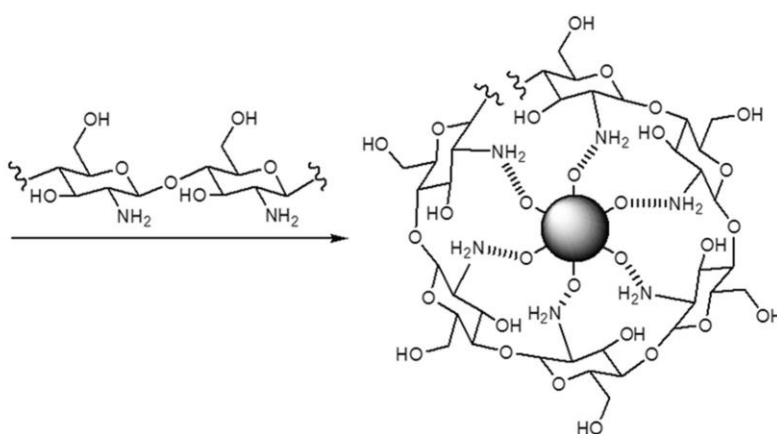


Fig 5. Chitosan stabilized SNPs³⁸.

Alginate is one of the natural polymers that have been investigated to study its effects when serving as a surfactant for SNPs as well as other nanoparticles, and has been found to improve biocompatibility and structural stability^{38,51}. Alginate is a polysaccharide with many carboxyl groups and it is speculated that COO⁻ of alginates and the positive iron ions on the surface of an SNP could stabilize the nanoparticle and additionally provide the electrostatic repulsion needed between each individual SNP to prevent aggregation thus keeping the nanoparticle stable⁴⁰.

Some of the standard methods of synthesis of alginate coated SNPs consist of three steps:

i) gelation of alginate and ferrous ions, ii) *in situ* precipitation of ferrous hydroxide by the alkaline treatment of alginate, and iii) oxidation of ferrous hydroxide with an oxidizing agent⁴⁰.

These methods can be complex and thus there has been research conducted to synthesize alginate stabilized nanoparticles in other ways.

SNPs stabilized by alginate were prepared by a two-step coprecipitation method. Here, the SNPs were 5-10 nm in diameter but had a hydrodynamic diameter of 193-483 nm. They showcased high T_2 relativities expected from iron oxide nanoparticles and thus were put forward as potential T_2 contrast agents⁷⁶. Another report describes the formation of egg-box like structure utilizing inter-connected alginate layers formed by the substitution of Na^+ present on Na-alginate with Ca^{2+} . This structure was placed in an Fe^{2+} solution after which it was oxidized to produce nanoparticles entrapped on the alginate *in situ* with mean sizes between 4.3 nm to 9.5 nm⁷⁷.

Another report discusses the pharmacokinetics and tissue distribution of alginate stabilized SNPs in Sprague-Dawley rats. The nanoparticles had a half-life of 0.27 hours when a concentration of 109.5 $\mu\text{mol Fe/kg}$ was used. Most of them were accumulated dominantly in the liver and the spleen likely due to them containing phagocytosing cells responsible for the removal of foreign material such as the SNPs⁷⁸.

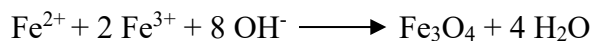
1.4 Synthesis of colloidal SNPs

Several methods have been reported for the synthesis of colloidal SNPs. These methods include co-precipitation, thermal decomposition, and polyol methods.

1.4.1 Co-precipitation

Co-precipitation is one of the most popular method that has been employed to synthesize iron oxide nanoparticles in aqueous solution^{40,79,80,81}. This method has been utilized since 1981 when Massart reported the synthesis of magnetic nanoparticles⁸². A challenge to co-precipitation synthesis is its optimization due to the particle formation mechanism not being entirely understood. This is because their formation is extremely rapid and can occur within seconds, thus providing an insufficient time to characterize initial precipitates⁸¹.

Co-precipitation employs iron precursors (Ferric/Ferrous ions) in a basic solution which is exposed to weak reducing agents such as NaOH, ammonia, and tetramethylammonium hydroxide (TMAOH). The ions are reduced to iron oxides at a temperature below 100 °C^{40,79,80,82}. The mechanism of the reaction is given by the equation:



The reaction pathway of the formation of iron oxide nanoparticles from their precursor molecules occurs through spontaneous nucleation, when the concentration of the species reaches critical supersaturation followed by a slow growth of the nuclei by diffusion of the solutes to the surface⁴⁰. All of this highly depends on pH strength, reducing agents and their addition rate, concentration of the precursors, temperature, and ionic strength⁸⁰. The complete precipitation of

Fe₃O₄ should be expected at pH = 8-14 in a non-oxidizing environment⁴⁰. Another factor to be considered is the use of surfactants discussed previously in this chapter, which can further yield additional differences in the type of SNPs produced. Several reports describe the formation of SNPs utilizing co-precipitation method^{83,84}.

1.4.2 Thermal decomposition

Thermal decomposition is a method that iron organic precursors such as Fe(Cup)₃, Fe(CO)₅, and Fe(acac)₃ are treated with heat until substances reach the temperature required to be decomposed (also known as the thermal decomposition temperature). The process itself is an endothermic reaction which requires heat to break the bonds between chemicals^{40,80}.

While the co-precipitation technique allows the rapid formation of SNPs, there can be some difficulty associated with the particle size distributions produced by co-precipitation and thermal decomposition attempts to overcome some of these limitations and can produce high quality of SNPs with a standard size^{79,80}. This is done because the SNP properties can be controlled by controlling the reaction time, the temperature, concentration ratios of the reactants, nature of the solvents, precursors, complexing strength and the addition of seeds. The SNPs themselves can be stabilized by a suitable surfactant being grafted on the surface of the nanoparticles⁴⁰.

Some factors that pose a challenge to thermal decomposition is perhaps industrial or large scale synthesis of the SNPs which can potentially impose a safety hazard due to the temperatures utilized for the formation of the SNPs which can reach temperatures above 300 °C⁴⁰, furthermore, addition of the surfactants to the SNPs at a large scale can pose a challenge

especially since some papers have utilized ligand exchange to stabilize the nanoparticles. Some methods for the synthesis of iron nanoparticles via thermal decomposition as well as improvements to the process have been published^{85,86}.

1.4.3 Polyol method

The polyol process is derived from another method of synthesis known as the sol-gel method^{40,82}. For the synthesis method, however, the polyol method utilized reduction, whereas the sol-gel method utilizes oxidation⁷⁹.

The polyol method is a versatile chemical method to synthesize nanoparticles as well as microparticles with well-defined shapes and sizes⁴⁰. A rather interesting feature in this method of nanoparticle synthesis are the solvents that are utilized, these are polyols (such as ethylene glycol, diethylene glycol, triethylene glycol, and polyethylene glycol^{40,82}). Owing to their dielectric constants, these solvents can dissolve inorganic compounds and have a significant room for temperature manipulation thus can work from room temperature to boiling point while simultaneously serving as reducing agents and stabilizers to assist with the control of nanoparticle growth as well as prevent their aggregation^{40,82}.

The process utilizes a precursor compound suspended in a liquid polyol that is stirred and heated at a suitable temperature, this begins the nucleation of the metal before forming particles the size of which can be controlled by increasing the reaction temperature, or by adding in foreign nuclei to inducing heterogeneous nucleation, this nucleation allows for the control of the particle size to an extent⁴⁰.

1.5 Stimuli-responsive nanoparticles for MRI

Stimuli-responsive (SR) nanoparticles have been widely investigated as efficient nanocarriers for drug/gene delivery^{87,88}. These ‘smart’ nanoparticles employ materials, both organic and inorganic, that can be activated by specific stimuli^{87,88}. Typical stimuli include pH, temperature, redox microenvironment, glutathione (GSH) and enzymes found in the body^{87,88,89,90,91,92}.

External stimuli such as radiation, ultrasound, and magnetic fields can also be used to trigger SR nanoparticles⁸⁸.

Zhaomin et al. described a novel redox-responsive star-shaped magnetic micelle with both active-targeted and magnetic-guided functions for cancer therapy illustrated in Fig 6. The micelles were formed through self-assembly of four-arm PEG and polycaprolactone (PCL) copolymers using disulfide bonds as intermediate linkers before having doxorubicin and SNPs physically encapsulated into the hydrophobic cores. The study indicated that the nanocarrier possessed anti-tumor efficacy under the application of an external magnetic field as doxorubicin was rapidly released under a high level of GSH to increase the concentration of drugs inside tumor cells.⁹³

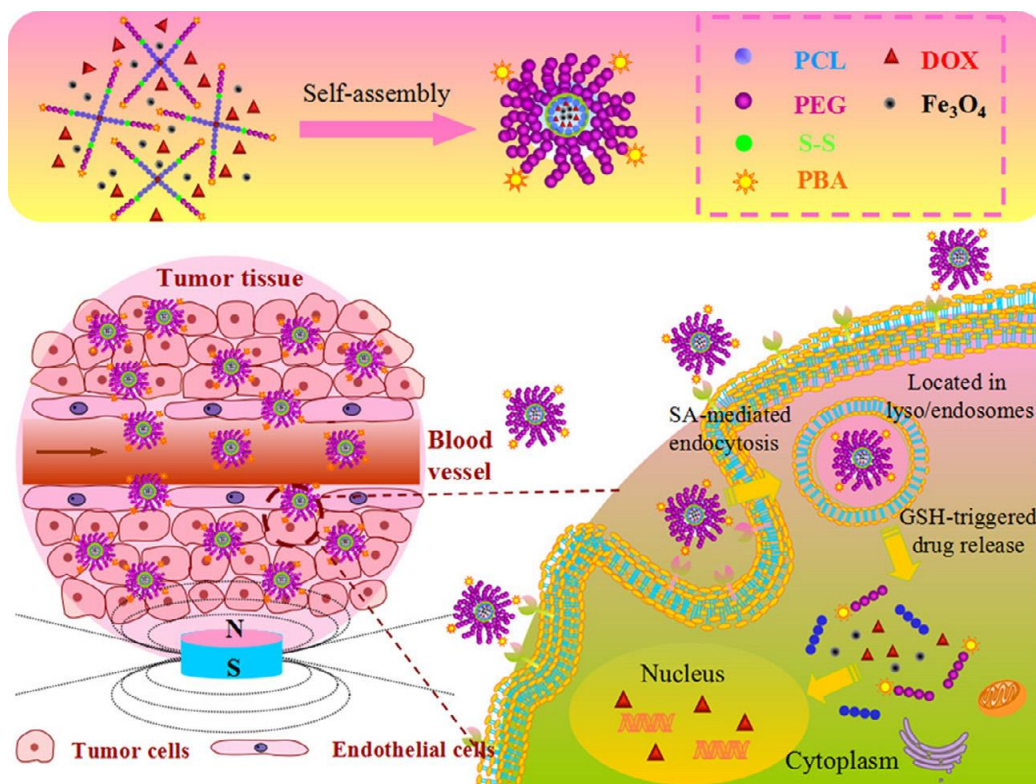


Fig 6. Schematic illustration of the fabrication of DOX-loaded magnetic star-shaped polymer micelles.⁹³

Most research involving SR nanoparticles was aimed at drug delivery nanocarriers, but many emerging papers describe SR nanoparticles with contrast enhancement or theranostic properties for MRI.

Cai et al described the development of a theranostic SNP drug delivery system for a sequential delivery of doxorubicin and zoledronic acid (ZOL) to breast cancer cells (Fig 7). This combination of chemotherapeutic agents was utilized to obtain an effective method of preventing advanced breast cancer and bone metastases by killing cancer cells. The SNPs remained stable in solution at 37 °C and physiological pH = (7.4). Increment of temperature via external magnetic fields or at low pH (5.0) in the presence of GSH stimulated a quick release of Dox followed by a

slow Zol release. Internalization of the nanoparticles by MCF-7 breast cancer cells allowed *in vivo* monitoring of the drug delivery.⁹⁴

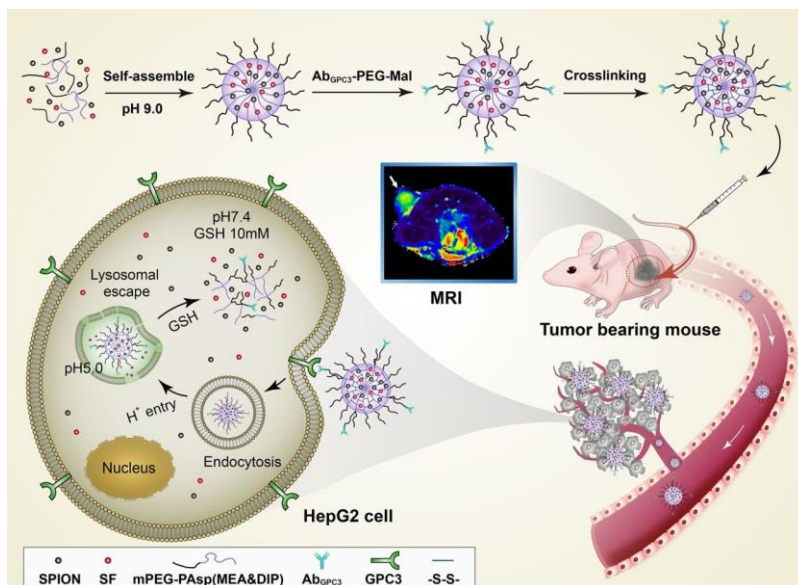


Fig 7. Schematic illustration of nanodrug preparation and dual-sensitive SF release in HepG2 cells⁹⁴.

Francisco et al describes the synthesis of biodegradable ligand-conjugated microparticles of iron oxides (MPIO) using the carboxy-NP and 29peptide-NP monomers. By using N-hydroxysulfosuccinimide ester in MES buffer amide linkages were formed between the monomers. The size of these MPIOs could be altered by changing the ratio of the two monomer types and could be degraded by endogenous clearance and degradation systems of the body such as enzymes. This degradable property suggested they could be potentially used as intravascular agents CAs for MRI⁹⁵.

Ma et al. reported a strategy to synthesize SNP clusters. SNPs with a diameter > 20 nm are more likely to accumulate in tumors than smaller ones due to limited extravasation into blood vessels after tumor uptake⁹⁶. Most T_1 SNP CAs had a diameter of 30 nm or smaller. A strategy to overcome the size limitations of SNPs and assist with better tumor accumulation was to synthesize appropriately sized USNP clusters. EDC coupling was used to react the citric acid's carboxyl groups on the surface of the USNPs with the dual amine groups of cystamine dihydrochloride (Cys). These clusters, due to their large size and enhanced interparticle interaction, showcased prominent T_2 MR effect before GSH induced reduction and formed single USNPs with T_1 MR effect, thus showcased a T_2 - T_1 effect. This is one of the first reported developments of redox-responsive clustered USNPs for convertible MR imaging of tumors for precision imaging of different biosystems⁹⁷.

Li et al mentioned the advantage of CA nanoparticles with a controlled assembly allow for a unique method to manipulate their collective magnetic properties thus influencing their MRI contrast effects. Their paper reported the formation of novel biocompatible ESNP clusters crosslinked by small molecular aldehyde derivative ligands (A_1) with potential use as T_1 CAs. Citric acid stabilized ESNPs underwent condensation reactions to form hydrazone bonds on their surface. A_1 was used to connect ESNPs through hydrazone bonds to form ESNP clusters, which are stable in neutral conditions but cleavable in acidic conditions. The rapid disassembly of the clusters to individual ESNPs in the acidic pH of tumor tissues causes a shift from T_2 relaxivity to T_1 relaxivity thus resulting in a T_2 to T_1 dual CA for the MRI as seen in Fig 8⁹⁸.

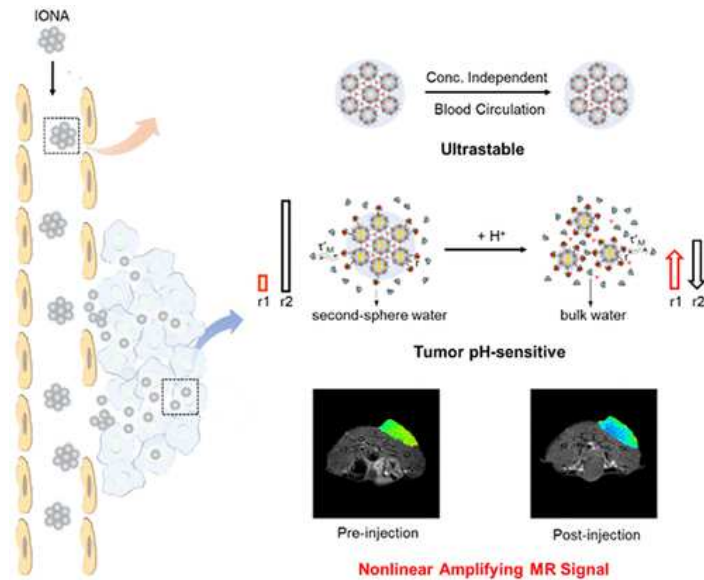


Fig 8. ESNP clusters disassembling into individual ESNPs due to the acidic environment of a tumor⁹⁸.

Lu et al describes T_2 - T_1 switching USNP clusters as SR CAs for MRI for the diagnosis of hepatocellular carcinomas (HCC) especially if less than 1 cm in size. USNPs with a core diameter of 3 nm were synthesized and covered with anchor pH-responsive i-Motif DNA that were cross-linked to form USNP clusters. Small HCC diagnosis was realized successfully by assembling USION clusters. The pH responsive i-motif-based linkers allowed the clusters acting as T_2 CAs to disassemble back into the T_1 CA upon encountering an acidic tumor microenvironment. In vivo, the clusters transformed in T_1 CAs at the HCC sites, while remaining unchanged in the Kupffer cells of normal liver tissue, where they functioned as T_2 CAs. The darkening of the normal liver and brightening of the HCC enabled highly sensitive diagnosis of small HCC.⁹⁹

Other approaches utilize micelles or nanogels to cluster SNPs. For example, Cao et al described ESIONPs stabilized with citric acid. The ESNPs were encapsulated in disulfide-crosslinked poly(carboxybetaine methacrylate) (poly(CBMA)) nanogels. Cyclo[Arg-Gly-Asp-D-Tyr-Lys] (c(RGD)) ligand was added to the nanogel for tumor-targeting as illustrated in Fig 9. This allowed for the conversion of NPs from T₂ to T₁ contrast in GSH rich environments such as tumor cells or tissue which were actively targeted. When the nanogel assembly was introduced into blood, a T₂ contrast effect was visible. Upon entry into cancer cells via c(RGD)-mediated endocytosis, the ESNPs were disassociated from the nanogel which resulted in a T₁ contrasting effect¹⁰⁰.

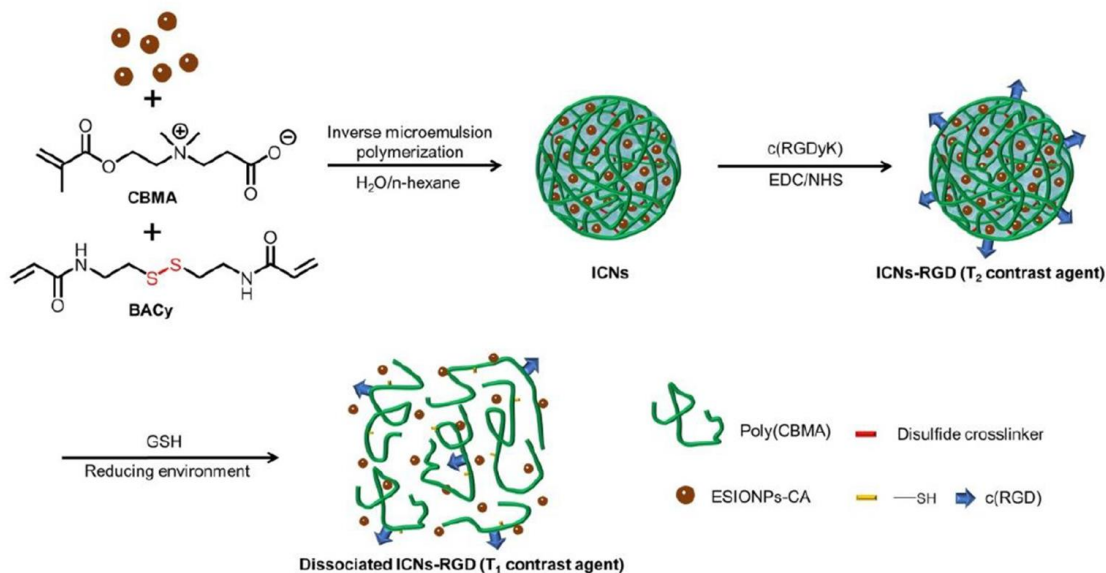


Fig 9. Scheme for preparation of ESNPs-packaged poly(CBMA) nanogels modified with c(RGD) ligand as an activatable MRI contrast agent with switchable function from a T₂ contrast agent to a T₁ one through the stimuli-responsiveness of GSH¹⁰⁰.

1.6 Scope of this thesis

This M.Sc research project is focused on the development of poly(acrylic acid) (PAA) stabilized USNPs crosslinked with disulfide bonds using cystamine to formulate SR USNP clusters as effective CAs for T₂-T₁ MRI application. This thesis consists of four chapters.

Chapter 1 introduces the history of MRI conception, its functions, and properties. Distinctions between CAs such as paramagnetic and superparamagnetic, and their properties are elaborated on. Methods to stabilize nanoparticles are discussed along with common types of stabilizers and their individual advantages. Commonly used methods for the synthesis of SNPs, and a brief overview of SR CAs for MRI are reviewed.

Chapter 2 covers instrumentation and analyses. The instrumentation for characterization of synthesized products and nanoparticles are mentioned along with their synthesis route. This chapter also includes the chemical reagents utilized and the strategy utilized for the synthesis of OA-USPNs, PAA-USPNs, SR PAA-USNP clusters.

Chapter 3 consists of the results and discussion. This includes the produced OA-USNPs and their properties, the properties of PAA stabilized USNPs and their comparison to OA-USNPs. Finally, the fabrication of SR PAA-USNP clusters and their degradation upon exposure to stimuli and their characterizations are discussed.

Chapter 4 consists of the conclusion and future work.

Chapter 2: Experimental

2.1 Instrumentation and analyses

Zeta potential (ζ) for aqueous PAA-stabilized-USNP colloids was measured using Zeta Potential Analyzer (Brookhaven) in aqueous solution at 25 °C.

Transmission Electron Microscopy (TEM) images were taken using a Philips Tecnai 12 TEM, operated at 120 kV and equipped with a thermionic LaB6 filament. An AMT V601 DVC camera with point-to-point resolution and line resolution of 0.34 nm and 0.20 nm respectively was used to capture images at 2048 by 2048 pixels. To prepare specimens, USNPs stabilized with OAs and PAA as well as PAA-USNP clusters in organic and aqueous solutions were dropped onto copper TEM grids (400 mesh, carbon coated) and then allowed to air dry at room temperature.

Dynamic light scattering (DLS) was used to determine hydrodynamic diameters by volume of USNPs stabilized with OAs and PAA as well as PAA-USNP clusters in organic and aqueous solutions at a fixed scattering angle of 175° at 25 °C with a Malvern Instruments Nano S ZEN1600 equipped with a 633 nm He-Ne gas laser.

Thermogravimetric analysis (TGA) measurements were carried out using a TA instruments Q50 analyzer. Typically, the dialyzed, heat dried samples (5-10 mg) were placed into a platinum pan and heated from 25 to 800 °C at a heating rate of 20 °C/min under nitrogen flow. The mass loss between 250 and 600 °C was used to calculate the USNP content in OA-USNPs/PAA-USNPs.

2.2 Materials

Ethanol (99%) (EtOH), chloroform, toluene, sodium hydroxide (NaOH), iron(II) chloride (FeCl_2 , 98%), iron(III) chloride (FeCl_3 , 97%), oleic acid (OA, 97%), DL-dithiothreitol (DTT). PAA (PAA MW = 2000 g/mol, 5000 g/mol and 8000 g/mol) from Sigma-Aldrich as well as. 1-ethyl-3-(3-dimethylaminopropyl) carbodiimide (EDC, >98%) and cystamine dihydrochloride (Cys, 97%) from Alfa Aesar were used as received.

2.3 Synthesis of OA-stabilized USNPs

OA-USNPs were synthesized as described in a previous publication¹⁰¹. A solution consisting of OA (13.6 g, 48 mmol), EtOH (36 mL), and toluene (63 mL) in a 250 mL three-necked round-bottom flask was degassed under nitrogen for 30 min. To the solution was added an aqueous solution of NaOH (1.92 g, 48 mmol) dissolved in water (12 mL) under a nitrogen atmosphere. A solution of FeCl_2 (0.76 g, 6 mmol) in water (5 mL) and an aqueous solution of FeCl_3 (1.95 g, 12 mmol) in water (10 mL) were separately prepared and degassed by nitrogen bubbling¹⁰¹. Both solutions were added to the solution using deoxygenated syringes. The combined mixture was stirred for 30 min at room temperature and then placed in an oil bath preset at 74 °C for 4 h. The black mixture was cooled to room temperature and then precipitated from EtOH. The precipitates were isolated by magnetic decantation, redispersed in hexane, and then centrifuged at 5000 rpm for 10 min to remove undissolved residues. The resulting supernatant in hexane was then precipitated from ethanol twice more to remove excess OA (not bound to USNPs)¹⁰¹. The synthesized OA-USNPs were stored in EtOH.

2.4 Fabrication of PAA-USNPs via ligand exchange

Biphasic ligand exchange was utilized for the fabrication of PAA-USNPs. OA-USNPs (20 mg, 3 mg/mL) dispersed in hexane (6 mL) were mixed with PAA (1.5 mg, 0.25 mg/mL) dissolved in an aqueous solution of EtOH (66 %, 6 mL) under stirring at 500 rpm for 24 hours at room temperature (RT). The organic phase was discarded. The aqueous phase containing the PAA-USNPs was collected and subjected to dialysis with dialysis tubing (12.4 kD MWCO) over aqueous 0.1 % NaOH solution (1 L) twice for 48 hours. The resultant PAA-USNPs were further purified by poly(ether sulfone) (PES) disk-type filters with 450 nm pore size.

2.5 Fabrication of SR PAA-USNP clusters by coupling reactions

The aqueous solution of PAA-USNPs was mixed with Cys in water (6 mL) under stirring at 500 rpm for 24 hours at RT to fabricate aqueous SR PAA-USNP clusters. The initial mole ratio of COOH: NH₂ was set to be 0.32:1 and increased to examine its effects on the fabrication of SR PAA-USNP clusters through EDC coupling reaction in aqueous solution. The concentration of EDC was kept at 0.07 mg/mL. The sample was collected and purified via dialysis using dialysis tubing (12.4 kD MWCO) over water for two days.

2.6 Reductive degradation of PAA-USNP clusters

The synthesized PAA-USNP clusters (2 mL) were mixed with DTT (1 mL, 25 mM) for 5 hours. Samples were taken for DLS and TEM analysis.

Chapter 3: Synthesis and reductive degradation of PAA-USNP clusters

3.1 OA-Stabilized USNPs (OA-USNPs)

USNP colloids stabilized with OA (OA-USNPs) were synthesized by co-precipitation in a mixture of water and toluene at 74 °C, according to the previous publications¹⁰¹. As-synthesized OA-USNPs were purified by precipitation from EtOH three times to remove excess OA molecules. The purified OA-USNPs dispersed in hexane were characterized for their size and morphology using DLS and TEM analysis. Fig 10a shows DLS diagrams of OA-USNP colloids that had a hydrodynamic diameter of 9 ± 0.6 nm which is close to 9.9 ± 0.2 nm in size as reported in the literature. The OA-USNPs synthesized are likely magnetite as illustrated by X-Ray diffraction (XRD) conducted by a publication utilizing a near identical co-precipitation method¹⁰². The XRD had peaks at 31.15° , 35.81° , 36.48° , 43.52° , 54.59° , 56.83° and 62.34° which are attributed to the crystal planes of magnetite at 220, 311, 222, 400, 422, 511 and 440, respectively.

Fig 10b shows TEM images and the core diameter of the OA-USNP nanoparticles was calculated to be 4.4 ± 1.0 nm using ImageJ software. Furthermore, OA-USNPs (BN-1) were characterized for their thermal properties using TGA. As seen in Fig 10c, the organic content (mostly OA molecules bound to USNP surfaces) were estimated as 37 wt% (i.e. 73 wt% of inorganic iron oxides) at 600 °C. Fig 10d shows the XRD pattern of magnetite nanoparticles.

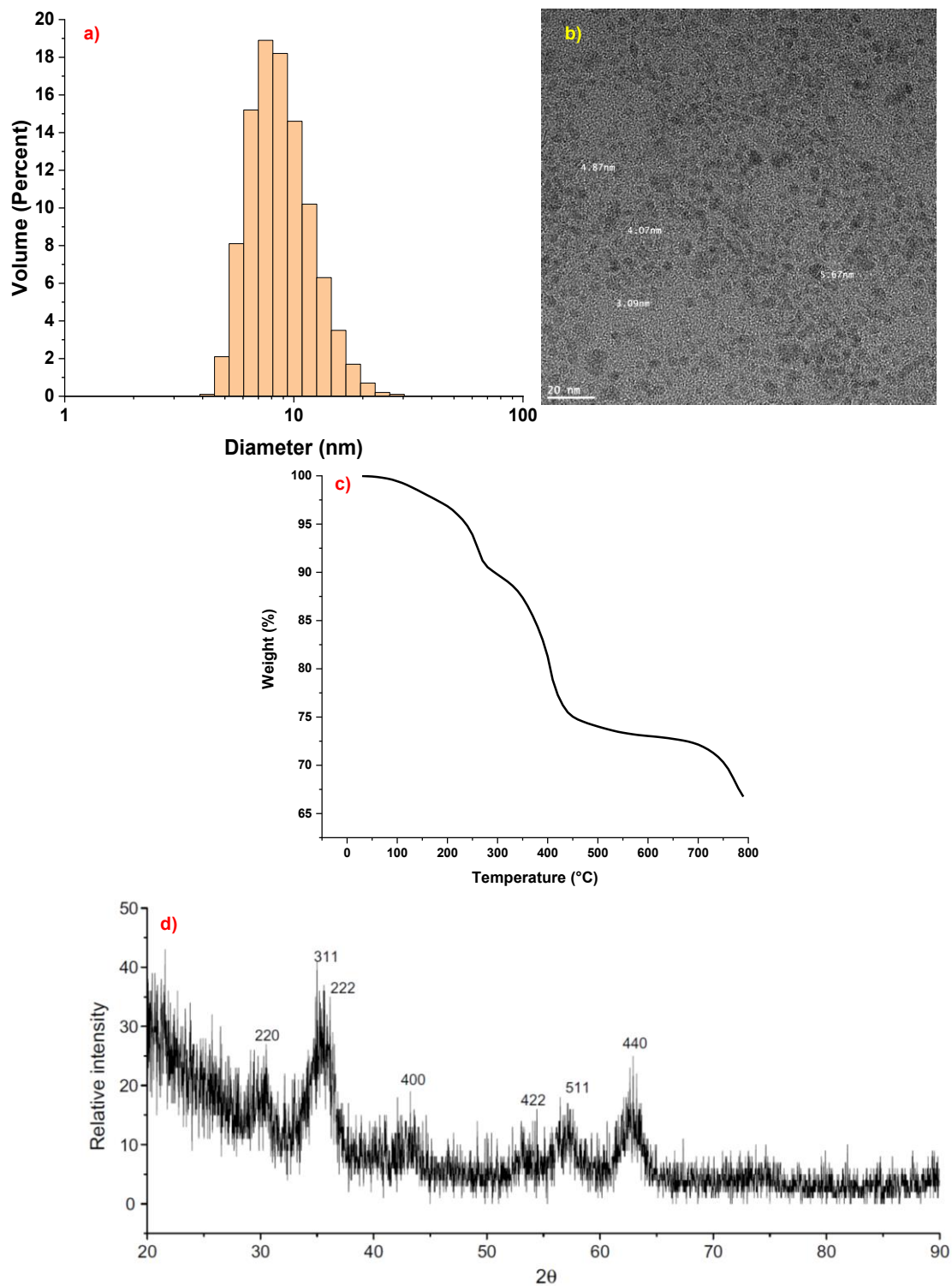


Fig 10. a) DLS diagram in hexane, b) TEM image, c) TGA thermogram, and d) XRD of magnetite OA-USNPs.

3.2 Fabrication of PAA-stabilized USNPs via biphasic ligand exchange

Biphasic ligand exchange were examined to fabricate aqueous PAA-USNP colloids with a single layer of PAA on USNP core. Our initial approach involves sonification. As illustrated in Fig 11, aliquots of OA-USNPs in hexane (0.04 mg/mL, 6 mL) were mixed with PAA in aqueous solution (1, 2 mg/mL, 6mL). The resulting biphasic mixtures were sonicated using a digital sonifier (Branson) for 40 min at 30% amplification. As described in literature¹⁰³. After sonication, the bottom layer (aqueous solution) was collected and analyzed by DLS technique.

DLS analysis shows a monomodal distribution with a diameter of 157 nm, which appears to be much larger than expected of single PAA-USNP colloid. Additionally, black precipitation was visible in the bottom of the vial. These results suggest the occurrence was due to excessive heat during sonification.

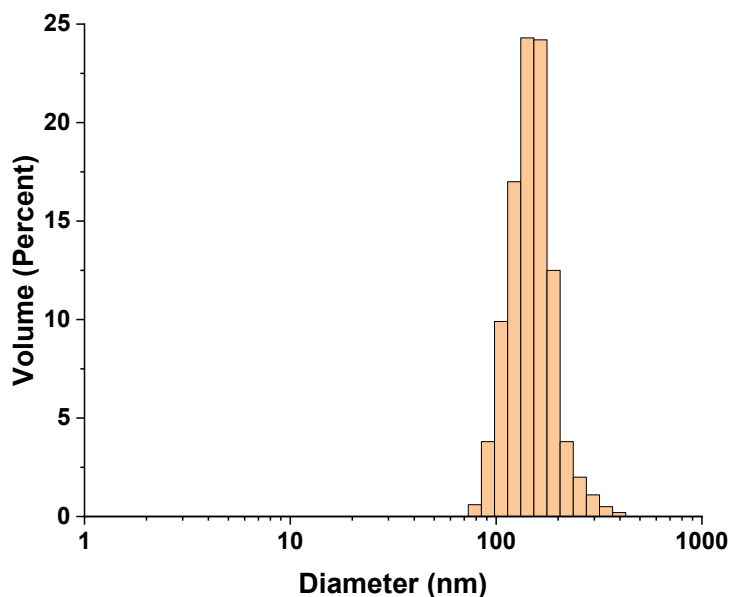


Fig 11. Illustration of the biphasic ligand exchange utilized to fabricate PAA-USNPs, followed by their purification.

Given the unexpectedly large aggregation through sonification, our approach was modified for biphasic ligand exchange at room temperature under stirring at 500 rpm for 24 hours. Using the modified approach, various parameters were examined to determine the best criteria for the fabrication of PAA-USNPs. These parameters include mass ratio of OA-USNPs with PAA as well as organic solvents if OA-USNPs (hexane vs chloroform) and mass ratio of water to EtOH of aqueous solution.

Initially, a higher amount of OA-USNPs was examined. In this experiment, OA-USNPs (> 100 mg) were dispersed in a) chloroform and b) hexane (Fig 12) and were mixed with PAA (500 mg) dissolved in aqueous solution (3 mL EtOH). The color of the aqueous layer turned brown, suggesting phase transfer of USNPs from organic to aqueous phase occurred. After purification by dialysis of aqueous solution, our DLS analysis shows the diameter to be ≥ 30 nm, but with a significant population of aggregates with a diameter of > 100 nm. Furthermore, a significant portion of OA-USNPs in the organic phase did not undergo ligand exchange, as was evident with dark brown coloration of the organic layer.

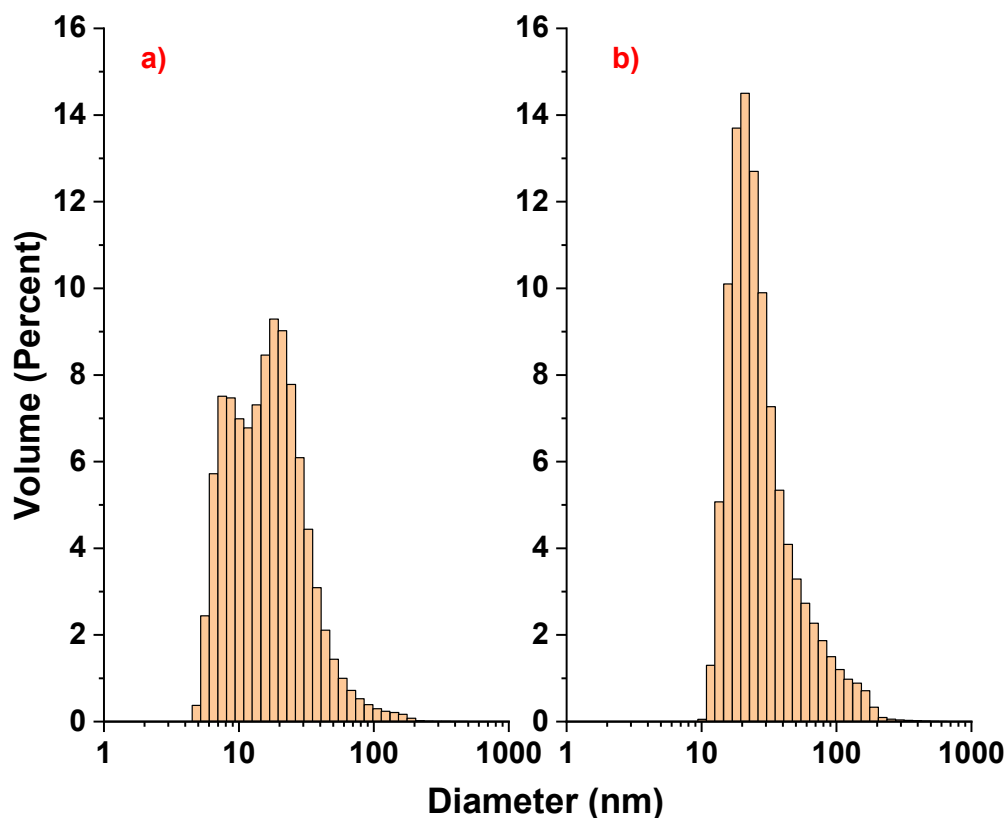


Fig 12. Illustration of biphasic ligand exchange utilized to fabricate PAA-USNPs using organic solvents a) chloroform b) hexane followed by their purification.

In the next experiments, the amount of OA-USNPs was reduced. OA-USNPs (20 mg, 3.3 mg/mL) dispersed in either hexane or chloroform were mixed with PAA (30 mg, 5 mg/mL) in aqueous solution (6 mL). Mass ratio of EtOH to water varied (82.5 %, 66 %, 33 %, 16.5 %). Pure EtOH wasn't examined to avoid the precipitation of OA-USNPs from organic solvent. Note that EtOH was used to purify OA-USNPs. The formed PAA-USNPs were purified using dialysis tubing for dialysis in aqueous 0.1% NaOH solution (1 L) twice over 48 hours. This process could remove excess PAA and any impurities including iron ions that might leach out of USNPs during ligand exchange when OA ligands were removed from the USNP surfaces. They were further purified by filtration with poly(ether sulfone) (PES) disk-type filters with 450 nm pore sizes to

eliminate larger aggregates of PAA-USNPs unexpectedly formed during ligand exchange. Our DLS analysis confirms that the diameter of PAA-USNPs formed 21 nm, 19 nm, 14 nm, 13 nm with 16.5 %, 33 %, 66 %, and 82.5 % EtOH in aqueous solution. This trend suggests that the diameter decreased with an increasing amount of EtOH in aqueous solution. (Fig 13)

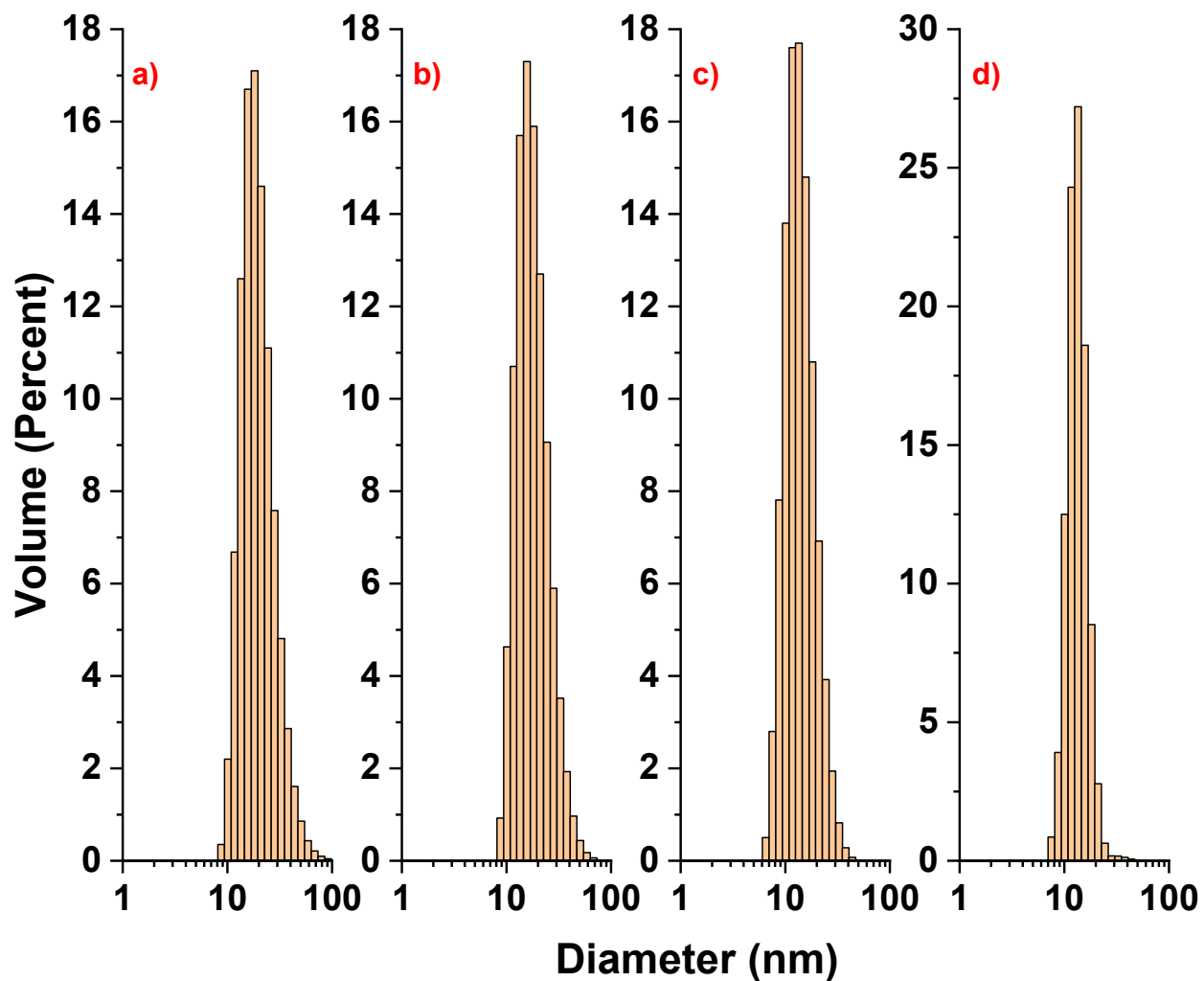


Fig 13. Illustration of fabricated PAA-USNP diameter decreasing ligand exchange with increased EtOH concentration (a) 16.5 % (b) 33 % (c) 66 % (d) 82.5 %.

OA-USNPs dissolved in both hexane and chloroform successfully underwent ligand exchange to fabricate PAA-USNPs. However, PAA-USNPs formed by biphasic ligand exchange utilizing chloroform had some degree of aggregation, no such aggregation was evident when using hexane as a solvent.

Fig 14 shows our size, morphology, and thermal properties of PAA-USNPs that were fabricated under in biphasic ligand exchange. OA-USNPs (20 mg, 3 mg/mL) dispersed in hexane (6 mL) were mixed with PAA (1.5 mg, 0.25 mg/mL) dissolved in an aqueous solution of EtOH (66 %, 6 mL) under stirring at 500 rpm for 24 hours at room temperature (RT). Following this, the organic phase was discarded. The aqueous phase containing PAA-USNPs was purified by dialysis using dialysis tubing (12.4 kD MWCO) over aqueous 0.1 % NaOH solution (1 L) twice for 48 hours. The resultant PAA-USNPs further purified by poly(ether sulfone) (PES) disk-type filters with 450 nm pore size.

Their core size of PAA-USNPs was determined to be 4.2 nm by TEM analysis, which is close to that of OA-USNPs counterparts. The inorganic content was determined as 35 % at 600 °C by TGA analysis. The PAA-USNP diameter (Fig 14) was 16 nm as analyzed by DLS.

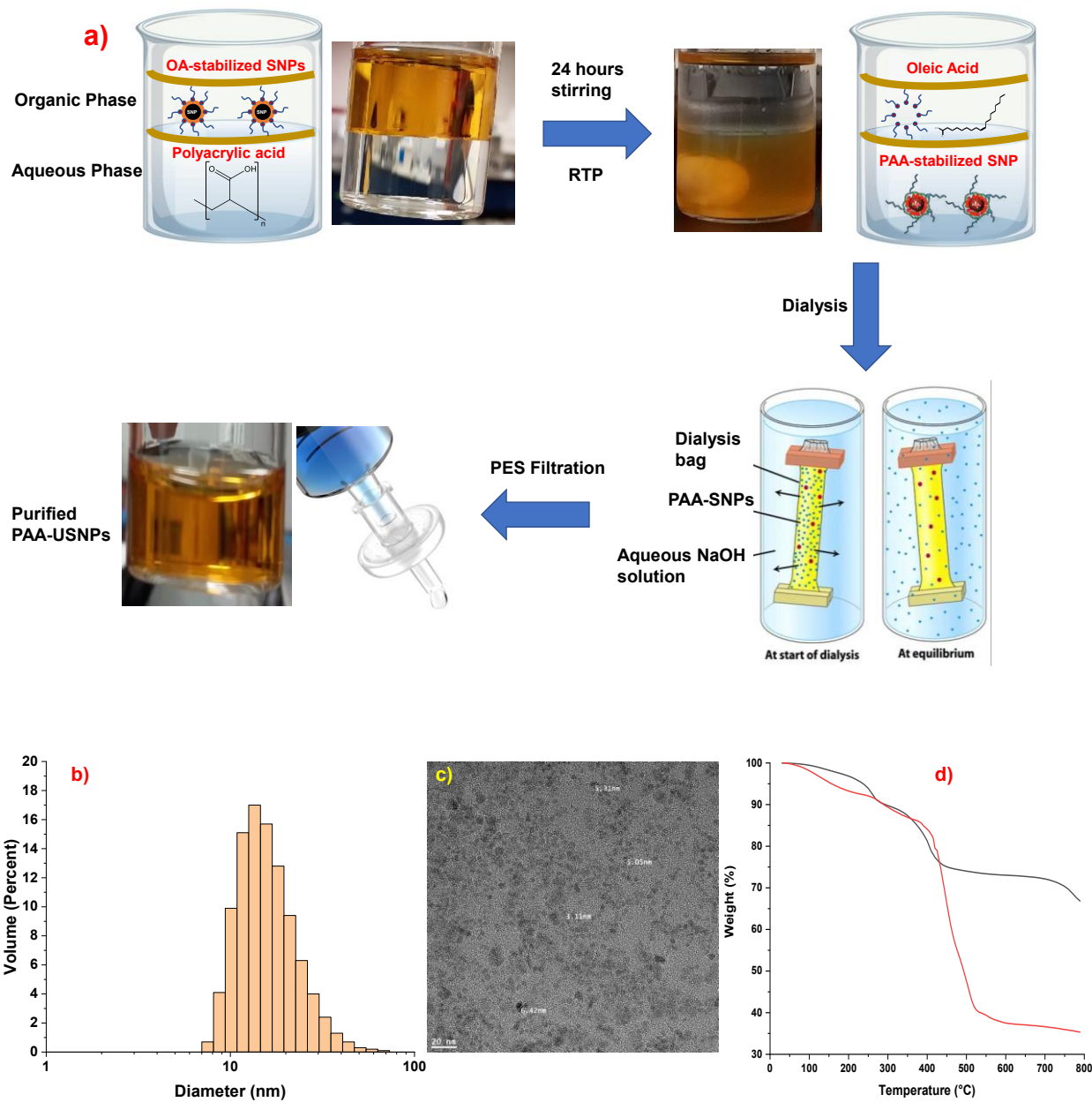


Fig 14. a) Schematic illustration of biphasic ligand exchange of OA-USNPs in hexane and PAA in aqueous phase, b) DLS diagram, c) TEM image, and d) TGA thermogram of PAA-USNP colloids.

3.2.1 Effect of molecular weight of PAA on ligand exchange

Andre et al reported that molecular weight of surfactants is an important parameter to influence the stability of nanoparticles *in vivo*¹⁰⁴. Where low molecular weight polymers can result in thin coatings that do not sufficiently screen van der Waals attractive forces, while high-molecular weight polymers bridge between particles, and insufficient polymer results in bare patches on the magnetite nanoparticle surfaces¹⁰⁴.

To investigate the molecular weight of PAA in our biphasic ligand exchange with OA-USNPs, molecular weight of PAA was varied with 2000, 5000, and 8000 g/mol. After being purified by dialysis method, the fabricated PAA-USNPs were characterized by DLS. As seen in Fig 15, the diameter of PAA-USNPs stabilized with PAA molecular weights 2000 g/mol, 5000 g/mol, and 8000 g/mol was 17 nm, 18 nm, and 20 nm respectively. This result suggests no significant effect of molecular weights of PAA on the fabrication of PAA-USNPs. However, it can be anticipated that they would have impact on colloidal stability and interactions with serum proteins *in vivo*.

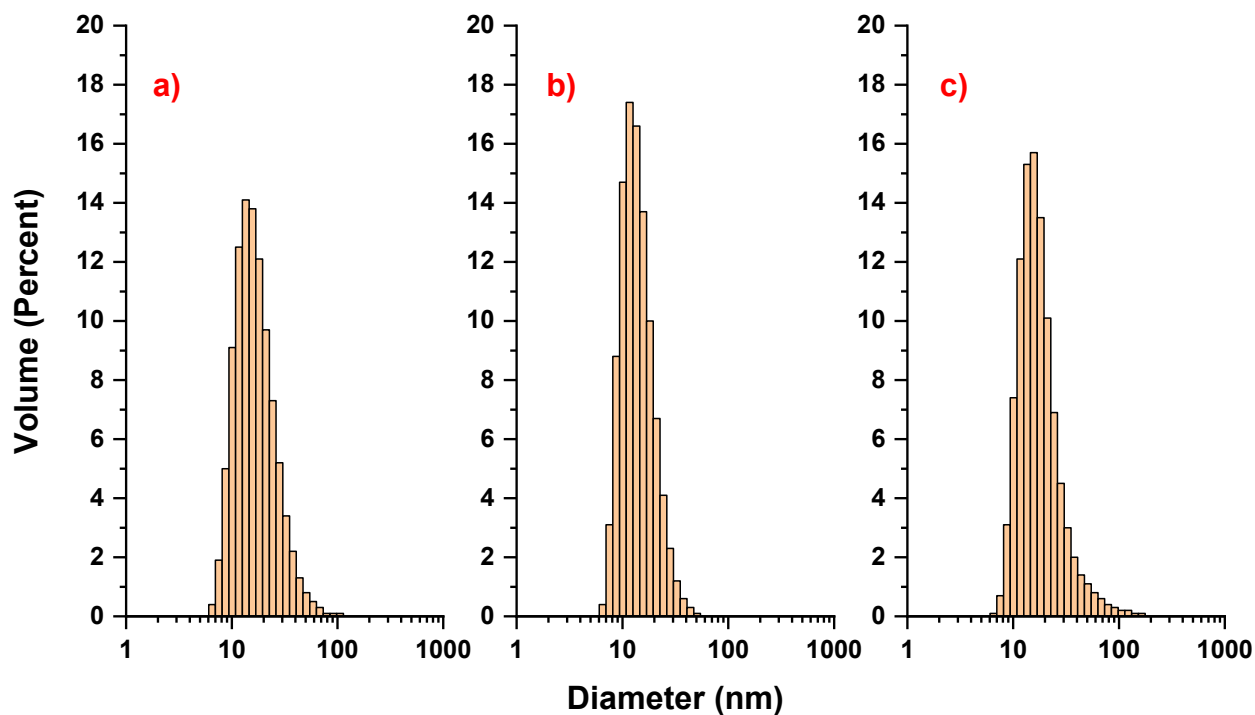


Fig 15. DLS diagrams of PAA-USNPs fabricated with PAA whose molecular weight is a) 2000, b) 5000, and c) 8000 g/mol.

3.3 Synthesis of SR PAA-USNP clusters via EDC coupling

Reductive PAA-USNP clusters labeled with disulfide linkages were fabricated by utilizing EDC coupling reactions of PAA-USNPs with Cys at room temperature. PAA on USNP surfaces has carboxylic acid (-COOH) groups that can be functionalized to introduce SR enhancements. Cys possesses disulfide linkages with terminal amino (-NH₂) groups which can react carboxylic acid groups present on the surface of USNPs to form amide linkages by optimizing coupling reactions (Fig 16).

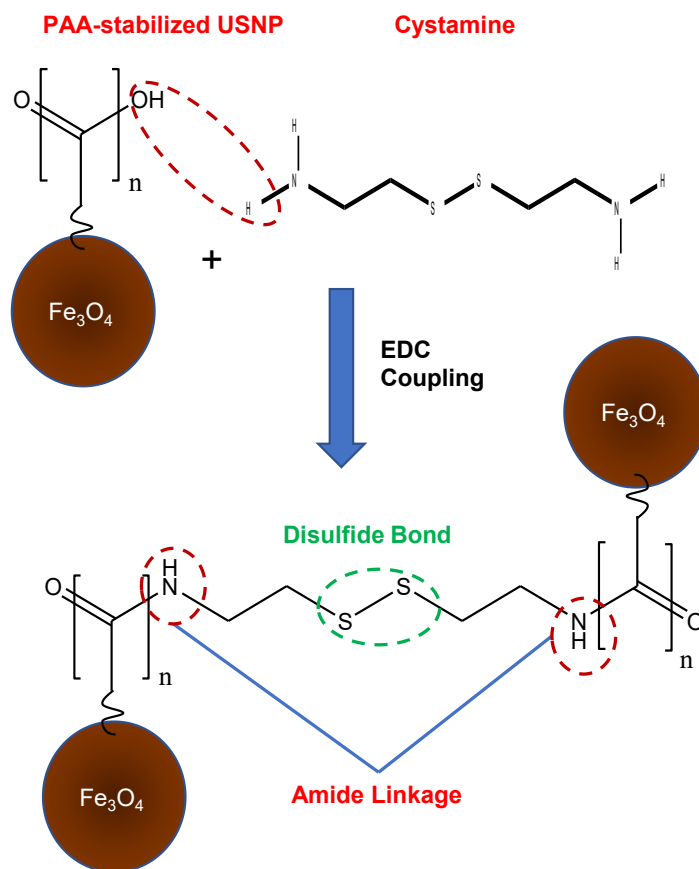


Fig 16. Illustration to fabricate SR PAA-USNP clusters through the formation of amide linkages by EDC coupling reactions of Cys with PAA-USNPs.

Disulfide bonds can be cleaved in response to reducing agents in a disulfide-thiol exchange reaction, some of these reducing agents include GSH which is found at significantly higher concentrations around cancer cells than normal healthy cells¹⁰⁵. This allowed binding of multiple PAA-USNPs to each other via Cys and introduced SR elements to the CA which can be triggered naturally in the presence of GSH or induced with the addition of a suitable reducing agent to disperse individual PAA-USNPs.

The amount of PAA-USNPs were kept constant (0.2 mg, 0.03 mg/mL) while the mass ratio of Cys:PAA was varied at (0.5:1, 1:1, and 2:1) in the presence of EDC, which corresponds to the mole ratios of NH₂: COOH to be 0.32:1, 0.64:1, and 1.28:1 respectively. The resulting mixtures in water were allowed to stir for 24 hours at 500 rpm at room temperature. They were subjected to dialysis over water for 24 hours and characterized by DLS. The successful formation of SR PAA-USNP clusters as evidenced with the presence of larger nanoparticles in DLS (Fig 17). The diameter of the formed clusters with Cys: PAA mass ratios of 0.5:1, 1:1, and 2:1 is 60 nm, 109 nm, and 124 nm respectively. Larger micron sized particles were observed. The results suggest that the EDC coupling reactions were successful in formulating SR PAA-USNP clusters whose size could be decreased or reduced by adjusting the ratio of NH₂: COOH used. The core size of PAA-USNP clusters in one batch was determined to be 4.13 ± 0.8 nm by TEM analysis using ImageJ software, which is close to that of individual PAA-USNPs.

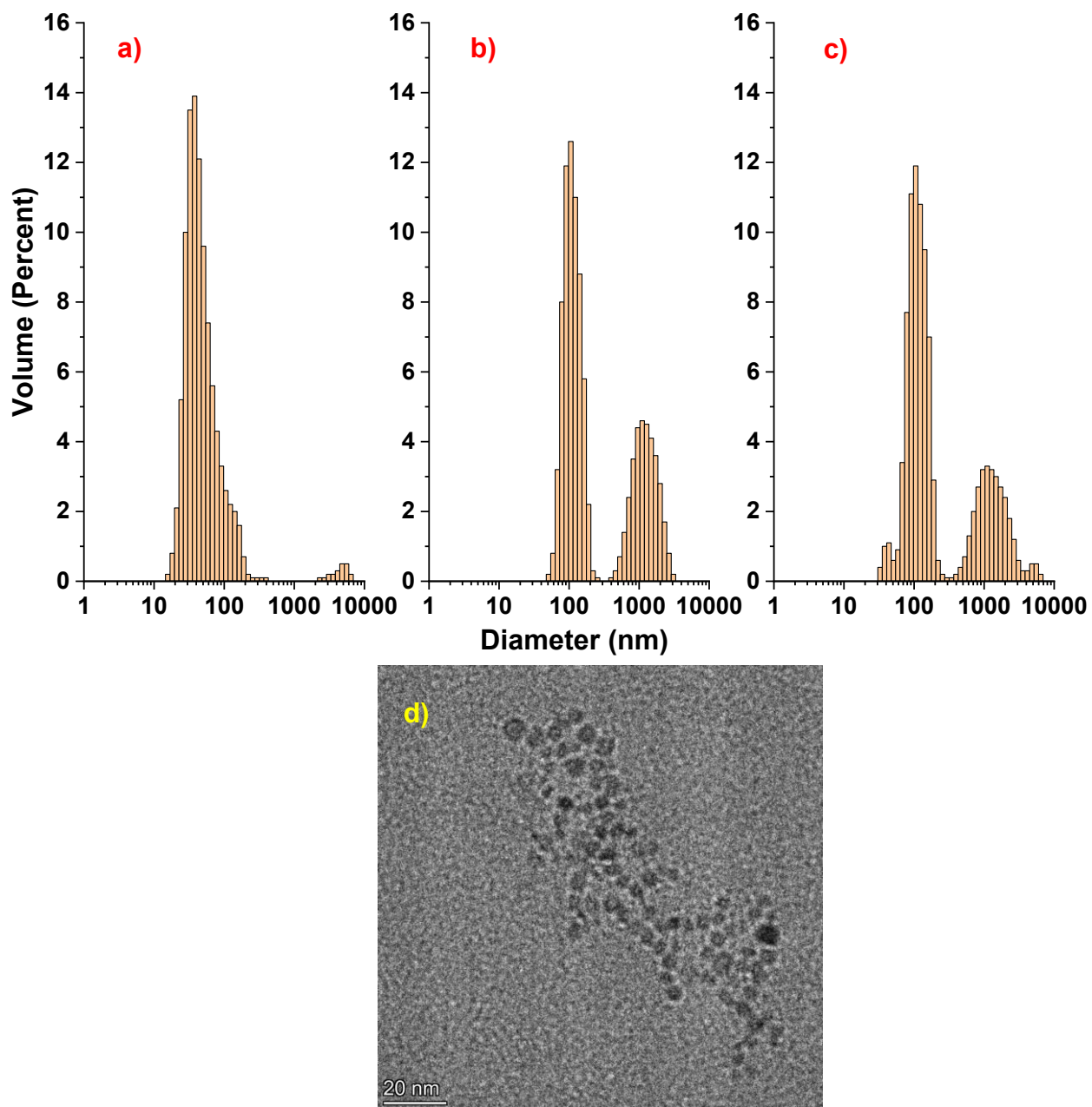


Fig 17. DLS diagrams of PAA-USNP clusters fabricated by altering NH_2 : COOH mole ratios to a) 0.32:1, b) 0.64:1, and c) 1.28:1 and d) TEM images of PAA-USNP clusters.

Some of the challenges utilizing this method for the formulation of SR PAA-USNP clusters can be that the samples produced can vary in size depending upon the PAA-USNP batch used. Furthermore, the sizes measured by the DLS are optimized for spherical nano-formulations, the shape of the clusters can be difficult to determine which could be potentially causing the size discrepancies in DLS.

3.4 Reductive degradation of SR PAA-USNP clusters

The formed PAA-USNP clusters are crosslinked with reductively cleavable disulfide bonds. In a reducing environment, the disulfide bonds could be cleaved, causing the degradation of the clusters to single PAA-USNP colloids. This process was followed by DLS measurements.

In the experiment, aliquots of PAA-USNP clusters with the diameter to be 60 nm (2 mL) were exposed to 0.25 M aqueous DTT solution (1 mL) for 5 hours. Fig 18 shows the DLS diagrams of clusters before and after treatment with DTT. Upon exposure to DTT, the diameter significantly decreased to 24 nm, which is very close to that (19 nm) of OA-USNPs used to fabricate PAA-USNPs. This result is promising to suggest the degradation of PAA-USNP clusters to single PAA-USNPs upon the cleavage of disulfide linkages in a reducing environment. The core size of degraded PAA-USNP clusters in one batch was determined to be 3.97 ± 0.7 nm by TEM analysis using ImageJ software, which is close to that of individual PAA-USNPs.

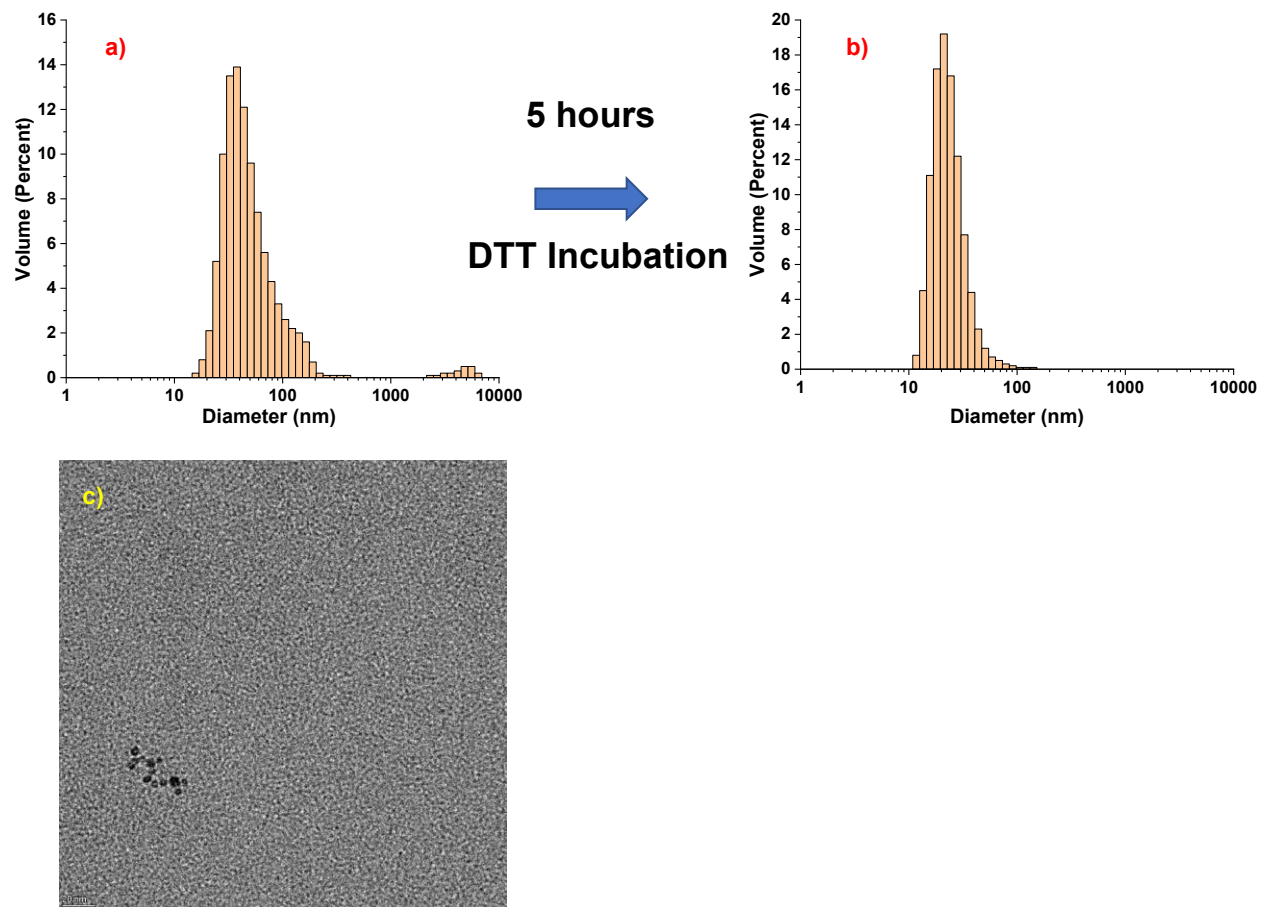


Fig 18. DLS diagrams of PAA-USNP clusters with diameter of 60 nm a) before and b) after treatment with DTT, and c) TEM image of PAA-USNP clusters after DTT degradation.

Chapter 4 Conclusion and Future Work

Co-precipitation method utilizing a mixture of water and toluene was used to synthesize OA-USNPs. Chapter 3 explored biphasic ligand exchange where OA-USNPs in hexane were mixed with aqueous PAA solution to fabricate aqueous PAA-USNP colloids with a single layer of PAA on USNP surfaces. PAA appeared to be an effective stabilizer to USNPs, thus fabricating PAA-USNPs with core diameter = 4.2 nm similar to their OA-USNP counterparts = 4.4 nm. The PAA-USNP diameter was < 30 nm which suggests their effectiveness as T₁ CAs for MRI. To form switchable T₂-T₁ clusters, reductive PAA-USNP clusters labeled with disulfide linkages were fabricated by utilizing EDC coupling reactions of PAA-USNPs with Cys. The resulting fabricated clusters were ≥ 67 nm in diameter and responsive to external reducing environments induced by GSH/DTT. The clusters dispersed into individual 24 nm PAA-USNPs as analyzed by DLS. These properties are promising in biomedical applications and are expected in case of switchable CAs for MRI.

Future work consists of further characterization of SR PAA-USNPs and their clusters. These include i) FTIR measurements to determine means of PAA fabrication on USNP surfaces; ii) relaxivity measurements the fabrications prior to clustering, post clustering, and post degradation; and iii) Ellman's assay to determine the concentration of disulfide bonds present on the fabricated clusters in order for an accurate appraisal of the moles of reducing agent required to stimulate degradation. Finally, *in vivo* experimentations are required to test the stability of the SR PAA-USNP clusters upon exposure to blood serums.

In conclusion, smart and responsive clusters were fabricated which show potential as dual imaging CAs for MRI.

References:

1. McRobbie, D. W., E. A. Moore, et al. (2006). MRI from Picture to Proton. Cambridge, Cambridge University Press.
2. Geva, T. (2006). "Magnetic Resonance Imaging: Historical Perspective." *Journal of Cardiovascular Magnetic Resonance* 8(4): 573-580.
3. CaseWesternReserveUniversity, school of medicine, MRI of the brain & spine: Basics
4. Huettel, S. A.; Song, A. W.; McCarthy, G. *Functional Magnetic Resonance Imaging*, 2nd ed.; Sinauer Associates: Sunderland, Mass., 2009.
5. Vlaardingerbroek, M. T. and J. A. den Boer (2003). *MRI and Its Hardware*. Magnetic Resonance Imaging: Theory and Practice. M. T. Vlaardingerbroek and J. A. den Boer. Berlin, Heidelberg, Springer Berlin Heidelberg: 9-54.
6. Strijkers J. Gustav, M. Mulder J. Willem, F. van Tilborg A. Geralda and Nicolay Klaas, *MRI Contrast Agents: Current Status and Future Perspectives, Anti-Cancer Agents in Medicinal Chemistry* 2007; 7(3).
7. de Haën, C. (2001). "Conception of the first magnetic resonance imaging contrast agents: a brief history." *Top Magn Reson Imaging* 12(4): 221-230.
8. Weinmann, H. J., et al. (1984). "Characteristics of gadolinium-DTPA complex: a potential NMR contrast agent." *AJR Am J Roentgenol* 142(3): 619-624.
9. Geraldès, C. F. and S. Laurent (2009). "Classification and basic properties of contrast agents for magnetic resonance imaging." *Contrast Media Mol Imaging* 4(1): 1-23.
10. Mao, X., et al. (2016). "Functional nanoparticles for magnetic resonance imaging." *Wiley Interdiscip Rev Nanomed Nanobiotechnol* 8(6): 814-841.

11. Wahsner, J., et al. (2019). "Chemistry of MRI Contrast Agents: Current Challenges and New Frontiers." *Chemical Reviews* 119(2): 957-1057.
12. Yan, G.-P., et al. (2007). "Magnetic resonance imaging contrast agents: Overview and perspectives." *Radiography* 13: e5-e19.
13. Xiao, Y.-D., et al. (2016). "MRI contrast agents: Classification and application (Review)." *Int J Mol Med* 38(5): 1319-1326.
14. Hao, D., et al. (2012). "MRI contrast agents: basic chemistry and safety." *J Magn Reson Imaging* 36(5): 1060-1071.
15. Pellico, J., et al. (2019). "Nanoparticle-Based Paramagnetic Contrast Agents for Magnetic Resonance Imaging." *Contrast Media Mol Imaging* 2019: 1845637.
16. Caravan, P., et al. (1999). "Gadolinium(III) Chelates as MRI Contrast Agents: Structure, Dynamics, and Applications." *Chemical Reviews* 99(9): 2293-2352.
17. Lohrke, J., et al. (2016). "25 Years of Contrast-Enhanced MRI: Developments, Current Challenges and Future Perspectives." *Adv Ther* 33(1): 1-28.
18. Murphy, K. J., et al. (1996). "Adverse reactions to gadolinium contrast media: a review of 36 cases." *American Journal of Roentgenology* 167(4): 847-849.
19. Marckmann, P., et al. (2006). "Nephrogenic systemic fibrosis: suspected causative role of gadodiamide used for contrast-enhanced magnetic resonance imaging." *J Am Soc Nephrol* 17(9): 2359-2362.
20. Dillman, J. R., et al. (2007). "Frequency and Severity of Acute Allergic-Like Reactions to Gadolinium-Containing IV Contrast Media in Children and Adults." *American Journal of Roentgenology* 189(6): 1533-1538.

21. Hunt, C. H., et al. (2009). "Frequency and severity of adverse effects of iodinated and gadolinium contrast materials: retrospective review of 456,930 doses." *AJR Am J Roentgenol* 193(4): 1124-1127.
22. Dillman, J. R., et al. (2008). "Allergic-Like Breakthrough Reactions to Gadolinium Contrast Agents After Corticosteroid and Antihistamine Premedication." *American Journal of Roentgenology* 190(1): 187-190.
23. Semelka, R. C., et al. (2016). "Gadolinium in Humans: A Family of Disorders." *American Journal of Roentgenology* 207(2): 229-233.
24. Wang, Y.-X. J., et al. (2001). "Superparamagnetic iron oxide contrast agents: physicochemical characteristics and applications in MR imaging." *European Radiology* 11(11): 2319-2331.
25. Lee, N. and T. Hyeon (2012). "Designed synthesis of uniformly sized iron oxide nanoparticles for efficient magnetic resonance imaging contrast agents." *Chemical Society Reviews* 41(7): 2575-2589.
26. Teja, A. S. and P.-Y. Koh (2009). "Synthesis, properties, and applications of magnetic iron oxide nanoparticles." *Progress in Crystal Growth and Characterization of Materials* 55(1): 22-45.
27. Shokrollahi, H. (2013). "Contrast agents for MRI." *Materials Science and Engineering: C* 33(8): 4485-4497.
28. Gandhi, S. N., et al. (2006). "MR Contrast Agents for Liver Imaging: What, When, How." 26(6): 1621-1636.
29. Shen, Z., et al. (2017). "Iron Oxide Nanoparticle Based Contrast Agents for Magnetic Resonance Imaging." *Molecular Pharmaceutics* 14(5): 1352-1364.

30. Lawaczeck, R., et al. (2004). "Superparamagnetic iron oxide particles: contrast media for magnetic resonance imaging." 18(10): 506-513.
31. Ohgushi, M., et al. (1978). "Dextran-magnetite: A new relaxation reagent and its application to T2 measurements in gel systems." Journal of Magnetic Resonance (1969) 29(3): 599-601
32. Anselmo, A. C. and S. Mitragotri (2015). "A Review of Clinical Translation of Inorganic Nanoparticles." Aaps j 17(5): 1041-1054.
33. Jeon, M., et al. (2021). "Iron Oxide Nanoparticles as T1 Contrast Agents for Magnetic Resonance Imaging: Fundamentals, Challenges, Applications, and Prospectives." 33(23): 1906539.
34. Malhotra, N., et al. (2020). "Potential Toxicity of Iron Oxide Magnetic Nanoparticles: A Review." Molecules 25(14).
35. Jain, T. K., et al. (2008). "Biodistribution, Clearance, and Biocompatibility of Iron Oxide Magnetic Nanoparticles in Rats." Molecular Pharmaceutics 5(2): 316-327.
36. Studart, A. R., et al. (2007). "Colloidal Stabilization of Nanoparticles in Concentrated Suspensions." Langmuir 23(3): 1081-1090.
37. Gupta, A. K. and M. Gupta (2005). "Synthesis and surface engineering of iron oxide nanoparticles for biomedical applications." Biomaterials 26(18): 3995-4021.
38. Salehipour, M., et al. (2021). "Recent advances in polymer-coated iron oxide nanoparticles as magnetic resonance imaging contrast agents." Journal of Nanoparticle Research 23(2): 48.
39. Bulte, J. W. M. and D. L. Kraitchman (2004). "Iron oxide MR contrast agents for molecular and cellular imaging." 17(7): 484-499.

40. Laurent, S., et al. (2008). "Magnetic Iron Oxide Nanoparticles: Synthesis, Stabilization, Vectorization, Physicochemical Characterizations, and Biological Applications." *Chemical Reviews* 108(6): 2064-2110
41. Rehana, D., et al. (2015). "Hydroxy, carboxylic and amino acid functionalized superparamagnetic iron oxide nanoparticles: Synthesis, characterization and in vitro anti-cancer studies." *Journal of Chemical Sciences* 127(7): 1155-1166.
42. Yu, S. and G. M. Chow (2004). "Carboxyl group (-CO₂H) functionalized ferrimagnetic iron oxide nanoparticles for potential bio-applications." *Journal of Materials Chemistry* 14(18): 2781-2786.
43. Godymchuk, A., et al. (2019). "Agglomeration of iron oxide nanoparticles: pH effect is stronger than amino acid acidity." *Journal of Nanoparticle Research* 21(10): 208.
44. Boyer, C., et al. (2010). "The design and utility of polymer-stabilized iron-oxide nanoparticles for nanomedicine applications." *NPG Asia Materials* 2(1): 23-30.
45. Thomas, L. A., et al. (2009). "Carboxylic acid-stabilised iron oxide nanoparticles for use in magnetic hyperthermia." *Journal of Materials Chemistry* 19(36): 6529-6535.
46. Soares, P. I. P., et al. (2014). "Effects of surfactants on the magnetic properties of iron oxide colloids." *Journal of Colloid and Interface Science* 419: 46-51.
47. The, M. R. T. (2004). Citrate-coated (184(th) variant) very small superparamagnetic iron oxide particles. *Molecular Imaging and Contrast Agent Database (MICAD)*. Bethesda (MD), National Center for Biotechnology Information (US).
48. Yee, C., et al. (1999). "Self-Assembled Monolayers of Alkanesulfonic and -phosphonic Acids on Amorphous Iron Oxide Nanoparticles." *Langmuir* 15(21): 7111-7115.

49. Tang, L. and J. Cheng (2013). "Nonporous Silica Nanoparticles for Nanomedicine Application." *Nano Today* 8(3): 290-312.
50. Stöber, W., et al. (1968). "Controlled growth of monodisperse silica spheres in the micron size range." *Journal of Colloid and Interface Science* 26(1): 62-69.
51. Wu, W., et al. (2008). "Magnetic Iron Oxide Nanoparticles: Synthesis and Surface Functionalization Strategies." *Nanoscale Research Letters* 3(11): 397.
52. Piao, Y., et al. (2008). "Designed Fabrication of Silica-Based Nanostructured Particle Systems for Nanomedicine Applications." 18(23): 3745-3758.
53. Ali Dheyab, M., et al. (2021). "Recent Advances in Synthesis, Medical Applications and Challenges for Gold-Coated Iron Oxide: Comprehensive Study." 11(8): 2147.
54. da Silva, G., et al. (2016). "Studies of the Colloidal Properties of Superparamagnetic Iron Oxide Nanoparticles Functionalized with Platinum Complexes in Aqueous and PBS Buffer Media." *Journal of the Brazilian Chemical Society* 00: 1-9.
55. Yang, H., et al. (2011). "Targeted dual-contrast T1- and T2-weighted magnetic resonance imaging of tumors using multifunctional gadolinium-labeled superparamagnetic iron oxide nanoparticles." *Biomaterials* 32(20): 4584-4593.
56. De Palma, R., et al. (2007). "Silane Ligand Exchange to Make Hydrophobic Superparamagnetic Nanoparticles Water-Dispersible." *Chemistry of Materials* 19(7): 1821-1831.
57. Caragheorghopol, A. and V. Chechik (2008). "Mechanistic aspects of ligand exchange in Au nanoparticles." *Physical Chemistry Chemical Physics* 10(33): 5029-5041.
58. Lattuada, M. and T. A. Hatton (2007). "Functionalization of Monodisperse Magnetic Nanoparticles." *Langmuir* 23(4): 2158-2168.

59. Gupta, A. K., et al. (2007). "Recent advances on surface engineering of magnetic iron oxide nanoparticles and their biomedical applications." 2(1): 23-39
60. Xue, W., et al. (2018). "Effects of core size and PEG coating layer of iron oxide nanoparticles on the distribution and metabolism in mice." International journal of nanomedicine 13: 5719-5731.
61. Khandhar, A. P., et al. (2017). "Evaluation of PEG-coated iron oxide nanoparticles as blood pool tracers for preclinical magnetic particle imaging." Nanoscale 9(3): 1299-1306.
62. García-Jimeno, S. and J. Estelrich (2013). "Ferrofluid based on polyethylene glycol-coated iron oxide nanoparticles: Characterization and properties." Colloids and Surfaces A: Physicochemical and Engineering Aspects 420: 74-81.
63. Yue-Jian, C., et al. (2010). "Synthesis, self-assembly, and characterization of PEG-coated iron oxide nanoparticles as potential MRI contrast agent." Drug Development and Industrial Pharmacy 36(10): 1235-1244.
64. Brullot, W., et al. (2012). "Versatile ferrofluids based on polyethylene glycol coated iron oxide nanoparticles." Journal of Magnetism and Magnetic Materials 324(11): 1919-1925.
65. Frazier, R. A., et al. (1997). "In Situ Surface Plasmon Resonance Analysis of Dextran Monolayer Degradation by Dextranase." Langmuir 13(26): 7115-7120.
66. Crepon, B., et al. (1991). "Enzymatic degradation and immunogenic properties of derivatized dextrans." Biomaterials 12(6): 550-554.
67. Josephson, L., et al. (1990). "A functionalized superparamagnetic iron oxide colloid as a receptor directed MR contrast agent." Magn Reson Imaging 8(5): 637-646.

68. Mahmoudi, M., et al. (2009). "Cytotoxicity of Uncoated and Polyvinyl Alcohol Coated Superparamagnetic Iron Oxide Nanoparticles." *The Journal of Physical Chemistry C* 113(22): 9573-9580.
69. Kayal, S. and R. V. Ramanujan (2010). "Doxorubicin loaded PVA coated iron oxide nanoparticles for targeted drug delivery." *Materials Science and Engineering: C* 30(3): 484-490.
70. Mahmoudi, M., et al. (2008). "Optimal Design and Characterization of Superparamagnetic Iron Oxide Nanoparticles Coated with Polyvinyl Alcohol for Targeted Delivery and Imaging." *The Journal of Physical Chemistry B* 112(46): 14470-14481.
71. Chastellain, M., et al. (2004). "Particle size investigations of a multistep synthesis of PVA coated superparamagnetic nanoparticles." *Journal of Colloid and Interface Science* 278(2): 353-360.
72. Huang, H. and X. Yang (2004). "Synthesis of Chitosan-Stabilized Gold Nanoparticles in the Absence/Presence of Tripolyphosphate." *Biomacromolecules* 5(6): 2340-2346.
73. Feng, B., et al. (2009). "Synthesis of monodisperse magnetite nanoparticles via chitosan-poly(acrylic acid) template and their application in MRI." *Journal of Alloys and Compounds* 473(1): 356-362.
74. Wang, C., et al. (2013). "Multifunctional chitosan magnetic-graphene (CMG) nanoparticles: a theranostic platform for tumor-targeted co-delivery of drugs, genes and MRI contrast agents." *Journal of Materials Chemistry B* 1(35): 4396-4405.

75. Shakil, M. S., et al. (2020). "In Vivo Toxicity Studies of Chitosan-Coated Cobalt Ferrite Nanocomplex for Its Application as MRI Contrast Dye." *ACS Applied Bio Materials* 3(11): 7952-7964.
76. Ma, H.-l., et al. (2007). "Preparation and characterization of superparamagnetic iron oxide nanoparticles stabilized by alginate." *International Journal of Pharmaceutics* 333(1): 177-186.
77. Morales, M. A., et al. (2008). "In situ synthesis and magnetic studies of iron oxide nanoparticles in calcium-alginate matrix for biomedical applications." *Materials Science and Engineering: C* 28(2): 253-257.
78. Ma, H. L., et al. (2008). "Superparamagnetic iron oxide nanoparticles stabilized by alginate: Pharmacokinetics, tissue distribution, and applications in detecting liver cancers." *International Journal of Pharmaceutics* 354(1): 217-226.
79. Yusefi, M., et al. (2020). "Preparation and Properties of Magnetic Iron Oxide Nanoparticles for Biomedical Applications: A Brief Review." *Journal of Advanced Research in Materials Science* 75: 10-18.
80. Samrot, A. V., et al. (2021). "A review on synthesis, characterization and potential biological applications of superparamagnetic iron oxide nanoparticles." *Current Research in Green and Sustainable Chemistry* 4: 100042.
81. Besenhard, M. O., et al. (2020). "Co-precipitation synthesis of stable iron oxide nanoparticles with NaOH: New insights and continuous production via flow chemistry." *Chemical Engineering Journal* 399: 125740.

82. Nawaz, M., et al. (2019). 2 - Magnetic and pH-responsive magnetic nanocarriers. Stimuli Responsive Polymeric Nanocarriers for Drug Delivery Applications. A. S. H. Makhoulf and N. Y. Abu-Thabit, Woodhead Publishing: 37-85.
83. Lin, S., et al. (2017). "Preparation of uniform magnetic iron oxide nanoparticles by coprecipitation in a helical module microchannel reactor." *Journal of Environmental Chemical Engineering* 5(1): 303-309.
84. Carmen Bautista, M., et al. (2005). "Surface characterisation of dextran-coated iron oxide nanoparticles prepared by laser pyrolysis and coprecipitation." *Journal of Magnetism and Magnetic Materials* 293(1): 20-27.
85. Yu, W. W., et al. (2004). "Synthesis of monodisperse iron oxide nanocrystals by thermal decomposition of iron carboxylate salts." *Chemical Communications*(20): 2306-2307.
86. Unni, M., et al. (2017). "Thermal Decomposition Synthesis of Iron Oxide Nanoparticles with Diminished Magnetic Dead Layer by Controlled Addition of Oxygen." *ACS Nano* 11(2): 2284-2303.
87. Ganta, S., et al. (2008). "A review of stimuli-responsive nanocarriers for drug and gene delivery." *Journal of Controlled Release* 126(3): 187-204.
88. Zhang, J., et al. (2022). "Stimuli-Responsive Nanoparticles for Controlled Drug Delivery in Synergistic Cancer Immunotherapy." 9(5): 2103444.
89. Torchilin, V. P. (2007). "Targeted pharmaceutical nanocarriers for cancer therapy and imaging." *Aaps j* 9(2): E128-147.
90. Shenoy, D., et al. (2005). "Poly(ethylene oxide)-modified poly(beta-amino ester) nanoparticles as a pH-sensitive system for tumor-targeted delivery of hydrophobic drugs:

- part 2. In vivo distribution and tumor localization studies." *Pharm Res* 22(12): 2107-2114.
91. Shenoy, D., et al. (2005). "Poly(ethylene oxide)-modified poly(beta-amino ester) nanoparticles as a pH-sensitive system for tumor-targeted delivery of hydrophobic drugs. 1. In vitro evaluations." *Mol Pharm* 2(5): 357-366.
92. Kommareddy, S. and M. Amiji (2005). "Preparation and evaluation of thiol-modified gelatin nanoparticles for intracellular DNA delivery in response to glutathione." *Bioconjug Chem* 16(6): 1423-1432.
93. Tang, Z., et al. (2016). "Redox-responsive star-shaped magnetic micelles with active-targeted and magnetic-guided functions for cancer therapy." *Acta Biomaterialia* 42: 232-246.
94. Cai, M., et al. (2020). "A reduction and pH dual-sensitive nanodrug for targeted theranostics in hepatocellular carcinoma." *Biomaterials Science* 8(12): 3485-3499.
95. Perez-Balderas, F., et al. (2017). "Covalent assembly of nanoparticles as a peptidase-degradable platform for molecular MRI." *Nature Communications* 8(1): 14254.
96. Huang, J., et al. (2010). "Effects of nanoparticle size on cellular uptake and liver MRI with polyvinylpyrrolidone-coated iron oxide nanoparticles." *ACS Nano* 4(12): 7151-7160.
97. Ma, D., et al. (2020). "Redox-Sensitive Clustered Ultrasmall Iron Oxide Nanoparticles for Switchable T2/T1-Weighted Magnetic Resonance Imaging Applications." *Bioconjugate Chemistry* 31(2): 352-359.

98. Li, F., et al. (2019). "Dynamically Reversible Iron Oxide Nanoparticle Assemblies for Targeted Amplification of T1-Weighted Magnetic Resonance Imaging of Tumors." *Nano Letters* 19(7): 4213-4220.
99. Lu, J., et al. (2018). "Highly Sensitive Diagnosis of Small Hepatocellular Carcinoma Using pH-Responsive Iron Oxide Nanocluster Assemblies." *Journal of the American Chemical Society* 140(32): 10071-10074.
100. Cao, Y., et al. (2020). "Extremely Small Iron Oxide Nanoparticle-Encapsulated Nanogels as a Glutathione-Responsive T1 Contrast Agent for Tumor-Targeted Magnetic Resonance Imaging." *ACS Applied Materials & Interfaces* 12(24): 26973-26981.
101. Xiao, W., et al. (2018). "Superparamagnetic Iron Oxide Nanoparticles Stabilized with Multidentate Block Copolymers for Optimal Vascular Contrast in T1-Weighted Magnetic Resonance Imaging." *ACS Applied Nano Materials* 1(2): 894-907.
102. Wen, X., et al. (2008). "Preparation of monodisperse magnetite nanoparticles under mild conditions." *Current Applied Physics* 8(5): 535-541.
103. Li, P., et al. (2015). "Mussel-Inspired Multidentate Block Copolymer to Stabilize Ultrasmall Superparamagnetic Fe₃O₄ for Magnetic Resonance Imaging Contrast Enhancement and Excellent Colloidal Stability." *Chemistry of Materials* 27(20): 7100-7109.
104. Ditsch, A., et al. (2005). "Controlled Clustering and Enhanced Stability of Polymer-Coated Magnetic Nanoparticles." *Langmuir* 21(13): 6006-6018.
105. Quinn, J. F., et al. (2017). "Glutathione responsive polymers and their application in drug delivery systems." *Polymer Chemistry* 8(1): 97-126.